Quaternary Science Reviews 140 (2016) 125–141

Contents lists available at ScienceDirect

Quaternary Science Reviews

journal homepage: www.elsevier.com/locate/quascirev

The timing of Mediterranean sapropel deposition relative to insolation, sea-level and African monsoon changes

K.M. Grant [a, *], R. Grimm [b], U. Mikolajewicz [b], G. Marino [a], M. Ziegler [c], E.J. Rohling [a, d]

[a] Research School of Earth Sciences, The Australian National University, Canberra, ACT 2601, Australia
[b] Max-Planck-Institute for Meteorology, Bundesstrasse 53, 20146 Hamburg, Germany
[c] Department of Earth Sciences, University of Utrecht, Budapestlaan 455, Utrecht 3584 CD, The Netherlands
[d] Ocean and Earth Science, University of Southampton, National Oceanography Centre, European Way, Southampton SO14 3ZH, UK

ARTICLE INFO

Article history:
Received 2 August 2015
Received in revised form
21 March 2016
Accepted 23 March 2016
Available online 4 April 2016

Keywords:
Eastern Mediterranean
Sapropels
African monsoon
Sea level
Ice sheets
Insolation
Precession
Meltwater pulses

ABSTRACT

The Mediterranean basin is sensitive to global sea-level changes and African monsoon variability on orbital timescales. Both of these processes are thought to be important to the deposition of organic-rich sediment layers or 'sapropels' throughout the eastern Mediterranean, yet their relative influences remain ambiguous. A related issue is that an assumed 3-kyr lag between boreal insolation maxima and sapropel mid-points remains to be tested. Here we present new geochemical and ice-volume-corrected planktonic foraminiferal stable isotope records for sapropels S1 (Holocene), S3, S4, and S5 (Marine Isotope Stage 5) in core LC21 from the southern Aegean Sea. The records have a radiometrically constrained chronology that has already been synchronised with the Red Sea relative sea-level record, and this allows detailed examination of the timing of sapropel deposition relative to insolation, sea-level, and African monsoon changes. We find that sapropel onset was near-synchronous with monsoon run-off into the eastern Mediterranean, but that insolation–sapropel/monsoon phasings were not systematic through the last glacial cycle. These latter phasings instead appear to relate to sea-level changes. We propose that persistent meltwater discharges into the North Atlantic (e.g., at glacial terminations) modified the timing of sapropel deposition by delaying the timing of peak African monsoon run-off. These observations may reconcile apparent model–data offsets with respect to the orbital pacing of the African monsoon. Our observations also imply that the previous assumption of a systematic 3-kyr lag between insolation maxima and sapropel midpoints may lead to overestimated insolation–sapropel phasings. Finally, we surmise that both sea-level rise and monsoon run-off contributed to surface-water buoyancy changes at times of sapropel deposition, and their relative influences differed per sapropel case, depending on their magnitudes. Sea-level rise was clearly important for sapropel S1, whereas monsoon forcing was more important for sapropels S3, S4, and S5.

1. Introduction

The Mediterranean basin is an ideal natural laboratory for understanding the dynamic interplay between key climatic and hydrological processes on a range of timescales. Over millennial and longer intervals, changes in global ice volume and African monsoon dynamics are both registered in eastern Mediterranean marine sediments (Rohling et al., 2014, 2015). Detailed understanding of how these processes interact and translate into sedimentary signals is far from complete, and first requires deeper insights into a characteristic feature of these sediments: the periodic deposition of organic-rich layers, or "sapropels", in the eastern basin (for overviews, see Rossignol-Strick, 1985; Rohling and Gieskes, 1989; Rohling, 1994; Emeis et al., 1996; Cramp and O'Sullivan, 1999; Rohling et al., 2015, and references therein).

The formation of these sapropels has been attributed to combinations of surface-water freshening, reduced deep-water ventilation, and increased export production (e.g., Rossignol-Strick et al., 1982; Rossignol-Strick, 1985; Rohling, 1994; Higgs et al., 1994; Emeis et al., 1996; Jorissen, 1999; Thomson et al., 1999; Mercone et al., 2001; Casford et al., 2003; Abu-Zied et al., 2008; Schmiedl et al., 2010). The main driver behind these processes was a relative increase in surface-layer buoyancy, and the mechanism behind

* Corresponding author.
E-mail address: katharine.grant@anu.edu.au (K.M. Grant).

http://dx.doi.org/10.1016/j.quascirev.2016.03.026
0277-3791/

this buoyancy forcing has long been attributed to monsoon-related freshwater inputs into the eastern Mediterranean in response to periodic northward shifts of the intertropical convergence zone (ITCZ). Such shifts were associated with minima in the precession cycle (hence maxima in boreal summer insolation), which caused the summer monsoon rain belt to intensify and migrate north over river catchments and North African wadi systems that drain into the eastern Mediterranean, including the Nile (e.g., Rossignol-Strick et al., 1982; Rossignol-Strick, 1985; Rohling, 1999; Rohling and De Rijk, 1999; Rohling et al., 2002, 2004; Larrasoaña et al., 2003; Scrivner et al., 2004; Bianchi et al., 2006; Marino et al., 2007, 2009; Osborne et al., 2008, 2010).

This accepted scenario of surface buoyancy forcing primarily due to African monsoon changes has recently been challenged for the most recent (early to middle Holocene) sapropel 'S1' (Grimm et al., 2015). Based on comprehensive simulations with a 3-dimensional ocean-circulation model coupled to a biogeochemical model and including a sediment module, Grimm et al. (2015) concluded that the evolution of deep-water anoxia prior to S1 formation was initiated by sea-level rise and sea surface warming, and that monsoon-related (i.e., freshwater and nutrient input) forcings were not the sole cause for S1 formation because simulated deep-water oxygen depletion started before the onset of enhanced monsoon run-off. However, the study also acknowledged that monsoon forcing potentially played a significant role in determining the vertical extent of anoxia during S1 deposition. These findings lead to the question of whether other sapropels were also intrinsically linked – at least in part – to episodes of global ice melt. If so, this would represent a paradigm shift to the common narrative of how sapropels were formed.

A link between sapropel formation and the melting of northern hemisphere ice sheets was proposed in early studies of Mediterranean sediments (e.g., Kullenberg, 1952; Olausson, 1961; Ryan, 1972). More recently, Troelstra et al. (1991) suggested that glacial meltwater contributed towards preconditioning the Mediterranean for sapropel formation by lowering surface-water salinities. They also suggested that this preconditioning process was interrupted by the cold Younger Dryas (YD) interval. Rohling (1994) substantiated these claims using a simple hydraulic model (based on Rohling and Bryden, 1994), by demonstrating that both monsoon-related freshwater forcing and deglaciation may have contributed to S1 formation. Rohling (1994) also suggested that a lag in S1 deposition relative to the nearest insolation maximum may relate to the YD, which would have interrupted the progressive deterioration of deep-water ventilation (hence anoxia) necessary for sapropel formation.

Observational datasets to resolve the monsoon-versus-deglaciation question must include high-resolution records of sapropel deposition, (east) African monsoon variability, and ice-volume/sea-level change on robust and chronologically consistent timescales. Such datasets have not been available until recently (Grant et al., 2012, 2014). A key issue in this respect is the fact that a widely accepted astronomically tuned timescale for Mediterranean sediments assumes a 3-kyr lag between precession minima and sapropel mid-points (Hilgen et al., 1993; Lourens et al., 1996, 2004). This assumption was derived from direct radiometric age constraints for sapropel S1 (e.g., Lourens et al., 1996; Mercone et al., 2000; Casford et al., 2007; De Lange et al., 2008). Ziegler et al. (2010a) argued that radiometrically dated oxygen isotope records derived from Chinese speleothems could be used as a tuning target for eastern Mediterranean sapropels, in order to test if the specific S1 phase relationship can be extrapolated to older sapropels. They found that the lag is variable for older sapropels but that on average the assumption of a ~3 kyr lag is a good approximation for the Late Pleistocene.

Here we examine the detailed timing of sapropel deposition relative to insolation, sea-level, and African monsoon changes, using highly resolved, co-registered signals (i.e., measured on the same sample suite) of monsoon-related run-off and sapropels S1, S3, S4 and S5 in eastern Mediterranean core LC21 (southeastern Aegean Sea; Fig. 1). These records have a radiometrically constrained chronology which has already been synchronised (Grant et al., 2012) with the Red Sea relative sea-level (RSL) record (Siddall et al., 2003, 2004; Rohling et al., 2009), so inferred phase relationships between sapropels, monsoon forcing, and sea-level changes are robust within quantified uncertainties. It has been demonstrated that the Red Sea RSL record closely approximates global (eustatic) sea-level variations (see discussion and glacial isostatic modelling in Grant et al., 2014), which in turn reflect global ice-volume variability on glacial-interglacial timescales. We can therefore use the tightly constrained relationships in our dataset to remove ice-volume effects from the LC21 $\delta^{18}O$ record of the planktonic foraminifer *Globigerinoides ruber* (white) ($\delta^{18}O_{ruber}$), to produce a robust, deconvolved climate and hydrological record for the eastern Mediterranean, which extends over the entire last glacial cycle. We also present new sediment geochemical records from core LC21 that accurately delineate its sapropel intervals. By examining timing relationships – on an internally consistent, U/Th-based chronology – between sapropel deposition and changes in sea level, insolation and African monsoon run-off, we seek to clarify current understanding of sapropel formation mechanisms under different glacial boundary conditions. It is important to emphasise here that current knowledge of sapropel formation is largely based on sapropel S1, followed by S5, because these are the most studied sapropels. Yet S1 was relatively weakly developed and was associated with lower insolation forcing, compared to other sapropels. Also, both S1 and S5 were deposited after large deglaciations. These sapropels are therefore not typical of all sapropels, hence the need to examine a range of sapropels with different magnitudes of the postulated forcings.

An additional incentive for more detailed study of the dynamics behind sapropel formation is the recent development of a method to reconstruct past sea-level changes using eastern Mediterranean sediments (Rohling et al., 2014). This method relies on the sensitivity of eastern Mediterranean seawater $\delta^{18}O$ to glacial-interglacial sea-level changes in the Gibraltar Strait. However, the conversion of Mediterranean $\delta^{18}O$ to sea level is not systematically straightforward, due to the periodic influx of ^{18}O-depleted monsoon run-off into the eastern Mediterranean. As a result, the Mediterranean sea-level method currently involves identifying sapropel intervals and removing them from the sea-level reconstruction. A better understanding of eastern Mediterranean $\delta^{18}O$ changes across sapropel intervals, as presented in this study, will therefore contribute towards improving the Mediterranean sea-level method.

2. Methods

2.1. Geochemical analyses

Scanning x-ray fluorescence (XRF) elemental analyses of the archive halves of sediment core LC21 (southern Aegean Sea, 35° 40′ N, 26° 35′ E; Fig. 2) were performed at the British Ocean Sediment Core Research Facility (BOSCORF) at the National Oceanography Centre, Southampton, using an Itrax XRF core scanner (Cox Analytical Systems, Gothenburg, Sweden). XRF data were collected every 0.5 mm down-core using a molybdenum tube set at 30 kV and 30 mA, and a sampling time of 40 s directly at the core surface. The exposed core surface was covered with a 4 μm thin SPEX Certi Prep Ultralene1 foil to avoid contamination of the XRF measurement unit and desiccation of the sediment. Subsequent sub-

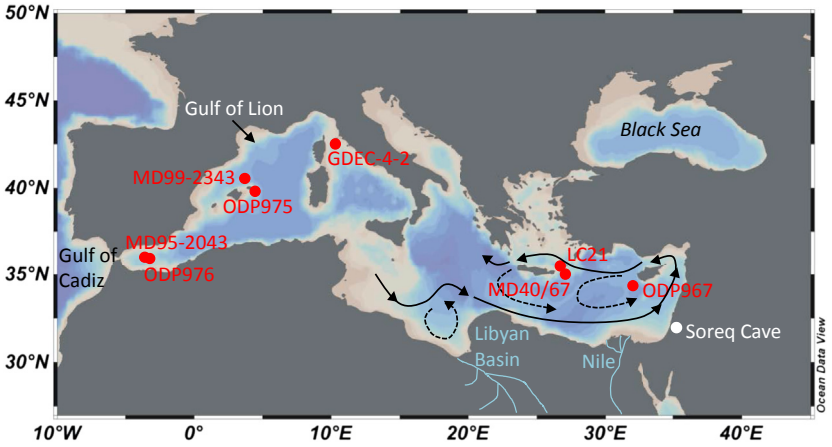

Fig. 1. Location of marine cores discussed in the study and schematic of surface circulation in the eastern Mediterranean Sea.

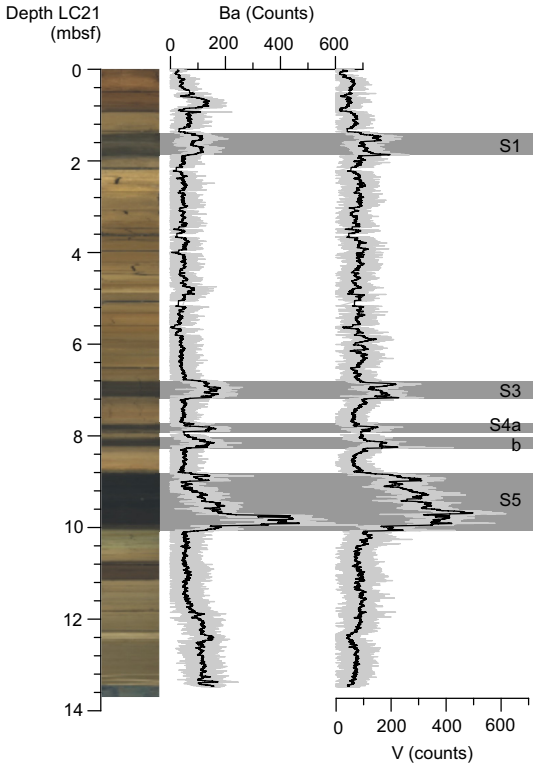

Fig. 2. Photograph of core LC21 (in metres below sea floor, mbsf) with scanning XRF records of barium and vanadium (grey, with 41-point moving averages in black). Sapropels are indicated (grey rectangles).

sampling at continuous 1-cm intervals and stable isotope analyses of the same core halves have been described in Grant et al. (2012). The foraminiferal stable oxygen and carbon isotope records discussed below are for the surface-dwelling species *Globigerinoides ruber* (white) ($\delta^{18}O_{ruber}$, $\delta^{13}C_{ruber}$) and the sub-surface dwelling species *Neogloboquadrina pachyderma* (dextral) ($\delta^{18}O_{pac}$, $\delta^{13}C_{pac}$) (cf. Rohling et al., 2004). Tests of these species were selected from >300 μm and 150–300 μm sieved sediment fractions, respectively (see Methods in Grant et al., 2012).

2.2. Sapropel boundaries

Four sapropels (S1, S3, S4, S5) are visibly identified in core LC21 by distinct colour and lithological changes, from olive-grey, fine-grained nannofossil ooze/clay admixtures to much darker layers rich in organic matter (sapropels) (Fig. 2). An 'interruption' to sapropel deposition is evident in S4 and to a lesser extent in S1 (Fig. 2). Because redox reactions at the sediment-seawater interface, and within sediments, can cause downward reduction at the sapropel base and downward oxidation (or 'burn down') at the sapropel top, sapropel boundaries are best identified using elements that are enriched in sapropels and that subsequently exhibit conservative behaviour within sediments (Thomson et al., 1995; De Lange et al., 2008). Barium is ideal for this purpose because it is well-preserved in sediments (Dymond et al., 1992), and enriched in sapropels (Thomson et al., 1995; De Lange et al., 2008) due to its association with export productivity (Dymond et al., 1992). In core LC21, pronounced increases in Ba at sapropel horizons are accompanied by elevated Vanadium (V). Vanadium is a redox-sensitive element and precipitates under reducing conditions, so although V can be mobile in sediments, the good agreement between increases in V and Ba in core LC21 implies that – in this case – elevated V reliably indicates sapropel boundaries (see Thomson et al., 1995; Nijenhuis et al., 1999; Table 1).

2.3. Chronology

The age-depth model for core LC21 is described in detail in Grant et al. (2012). Briefly, it is constrained by 14 direct radiocarbon datings and two geochemically 'fingerprinted' tephra layers (the Minoan and Campanian Ignimbrite; Satow et al., 2015) for the interval 0–40 ka BP, and by process-based correlation to the U/Th-dated Soreq Cave (Israel) speleothem $\delta^{18}O$ record for the interval >40–150 ka BP. All tie-points, radiometric ages (including all Soreq

Table 1
Age boundaries, duration [kyr, in parentheses] and mid-point of core LC21 sapropels, and timing of the respective monsoon signal.

Age: (ka BP)	Sapropel		Sapropel mid-point	Monsoon onset
S1	6.1–10.5	[4.4]	8.3	10.8
S3	80.8–85.8	[5.0]	83.3	85.8
S4	101.8–107.8	[6.0]	104.8	108.0
S4 interruption	*104.0–105.4*	*[1.4]*	*104.9*	
S5	121.5–128.3	[6.8]	124.9	128.3

speleothem datings) and their uncertainties were probabilistically assessed in a Bayesian deposition model (using 'OxCal' software, Bronk Ramsey, 2008, 2009). Full error propagation yielded age uncertainties (at 2σ) of 0.4 ± 0.2 kyr for the interval 0–40 ka BP, and 2.0 ± 0.9 kyr for the interval >40–150 ka BP. The Red Sea RSL record was synchronised with the LC21 chronology using the LC21 $\delta^{18}O_{pac}$ record (Grant et al., 2012); this record primarily reflects glacial-interglacial sea-level changes due to a 'glacial concentration' effect on Mediterranean seawater $\delta^{18}O$ similar to that in the Red Sea (see Rohling, 1999; Grant et al., 2012; and Rohling et al., 2014 for more technical details).

3. Deconvolving the LC21 $\delta^{18}O_{ruber}$ record

3.1. Global ice-volume effects

As mentioned before, global ice-volume changes strongly affect Mediterranean seawater $\delta^{18}O$ due to the restriction of exchange flow through the Strait of Gibraltar with lowering of sea level (Rohling, 1999; Rohling et al., 2014). The LC21 $\delta^{18}O$ records therefore contain an important sea-level component (equations (1) and (2)); removal of this component from the $\delta^{18}O_{ruber}$ record – a proxy for eastern Mediterranean surface-water $\delta^{18}O$ – will therefore isolate local climatic influences on Mediterranean surface-water $\delta^{18}O$ (see below). Calculation of this 'residuals' signal first requires conversion of the Red Sea relative sea-level (RSL) record (y) into equivalent eastern Mediterranean $\delta^{18}O$ values (x), based on the upper (equation (1)) and lower (equation (2)) probability limits for a quadratic relationship determined by Rohling et al. (2014):

$$y = 18.23253367 - 54.32756406x + 2.68013962x^2 \quad (1)$$

$$y = -19.83859107 - 54.97329064x + 1.027303677x^2 \quad (2)$$

Because the Red Sea RSL record is unreliable ca 14–23 ka BP (Fig. 3a; see Rohling et al., 2009), we have additionally converted into equivalent Mediterranean $\delta^{18}O$ values the probabilistic sea-level record of Stanford et al. (2011) for the last deglaciation (this record is based on numerous radiometrically dated sea-level indicators). The converted RSL records (Fig. 3a) were normalised to the Late Holocene values for $\delta^{18}O_{ruber}$ and then subtracted from $\delta^{18}O_{ruber}$. The resultant 'LC21 residuals' are defined by $\delta^{18}O_{ruber}$ values lighter/heavier than the upper/lower 95% probability intervals of the converted RSL records (Fig. 3b). While these probability intervals should account for most of the sea-level/ice-volume component in the $\delta^{18}O_{ruber}$ record, we note that there may be two short-term intervals (Section 3.2 below) where glacial influences on Mediterranean $\delta^{18}O$ have not been captured in the $\delta^{18}O$-to-sea-level conversion.

3.2. Meltwater effects

Observational data and numerical modelling both suggest that the flow of Atlantic water into the Mediterranean was significantly increased during glacial and deglacial North Atlantic freshening events, or 'Heinrich Stadials' (HS), compared to background conditions (e.g., Cacho et al., 1999; Sierro et al., 2005; Rogerson et al., 2010). Sierro et al. (2005) demonstrated that the past five HS were associated with significant ^{18}O depletions in western Mediterranean surface waters, after correcting the foraminifera $\delta^{18}O$ for temperature and ice-volume effects. These depletions were observed in the Alboran Sea (core MD95-2043) as well as north of the Balearic Islands (core MD99-2343) (Fig. 1). Subsequent studies have corroborated these findings. A western Mediterranean surface water ^{18}O depletion during HS has been documented for: the Gulf of Cadiz during HS1 (Voelker et al., 2006), the Strait of Sicily during HS1 (Essallami et al., 2007), the Gulf of Lion during HS1, HS2 and the YD (Melki et al., 2009; Lombo-Tombo et al., 2015), the Menorca Rise (ODP site 975) during HS11 (Kandiano et al., 2014), and the Alboran Sea (ODP site 976) during HS1 and HS11 (Jiménez-Amat and Zahn, 2015) (Fig. 1). Moreover, a synthesis of surface water $\delta^{18}O$ profiles from sediment cores from the Gulf of Cadiz and Alboran Sea covering the last ~30 ky revealed a reduced Atlantic-Mediterranean $\delta^{18}O$ gradient during HS (Rogerson et al., 2010). In the same study, a one-dimensional hydraulic control model for the Strait of Gibraltar confirmed that enhanced Atlantic inflow to the Mediterranean would result from a freshening of the North Atlantic associated with iceberg meltwater. Such a scenario has recently been corroborated by hosing experiments with a suite of CMIP5 models (Swingedouw et al., 2013), which show that (isotopically light) meltwater from the subpolar North Atlantic is directed towards the Gulf of Cadiz by the Canary current.

Comparison of the LC21 residuals with a record of sea-level change rates ('dRSL') on the same LC21 chronology, and with the (radiometrically dated) timing of meltwater pulse 1a (Deschamps et al., 2012) and HS1 (Álvares-Solas et al., 2011), and with the radiometrically constrained timing of HS11 (Marino et al., 2015) (Fig. 3c), reveals that the timing of large melting events during terminations I and especially II coincides with distinct intervals of negative residuals. The timing of HS3 and HS5 can also potentially be correlated with pronounced negative LC21 residuals ca 28–30 and 46–48 ka, respectively (Fig. 3b), in line with Sierro et al.'s (2005) observations of surface-water ^{18}O depletions in the western Mediterranean during the last five HS. This inference is possibly supported by dRSL for HS5, but not for HS3 (Fig. 3c).

If we consider sub-surface $\delta^{18}O$ records from core LC21 and ODP site 975 that have been tuned to the same age model (Marino et al., 2015; Figs. 1 and 4a), we observe an isochronous ^{18}O depletion at these sites during HS11. Although on a different age model, a depletion of similar timing and magnitude at ODP site 975 is recorded by surface-water $\delta^{18}O$ records (Kandiano et al., 2014; Fig. 4b), so the LC21 ^{18}O depletion appears to be consistent with widespread observations from the western Mediterranean. In that case, it seems likely that negative spikes in the LC21 residuals during major deglaciation events are due to North Atlantic (meltwater-related) $\delta^{18}O$ anomalies propagating into the eastern Mediterranean, and these short-term signals are not captured by the RSL-to-$\delta^{18}O$ conversion for the Mediterranean (Rohling et al., 2014).

An additional consideration is the direct input of glacial meltwater into the Mediterranean from alpine deglaciation and/or retreat of the European ice sheet (EIS). Regarding alpine meltwater, a synthesis of Mediterranean mountain glacial activity suggests that the last deglaciation was staggered, with several glacial advances/retreats occurring between the last glacial maximum and the Holocene, yet there are no reliably dated records from many areas (see Hughes and Woodward, 2009). The relatively small glaciers in this region would have responded rapidly to climate change and decayed much faster than extensive ice sheets (Hughes et al., 2006), which implies that the largest meltwater effects on Mediterranean $\delta^{18}O$ would have occurred early in the deglaciation. It therefore seems unlikely that the negative LC21 residuals ca 15 ka are primarily due to alpine meltwater. Nonetheless, a negative shift in surface water $\delta^{18}O$ coinciding with HS1 has been recorded in cores from the Rhone Canyon, in the far north Gulf of Lion (Lombo Tombo et al., 2015), which may reflect enhanced Rhone run-off at that time. Also, Rohling et al. (2015) argued that alpine meltwater from the Rhone offered the most plausible explanation for the onset of the most recent organic rich layer (ORL1) in the western Mediterranean, at ~14.5 ka.

Even less information about Mediterranean alpine meltwater is

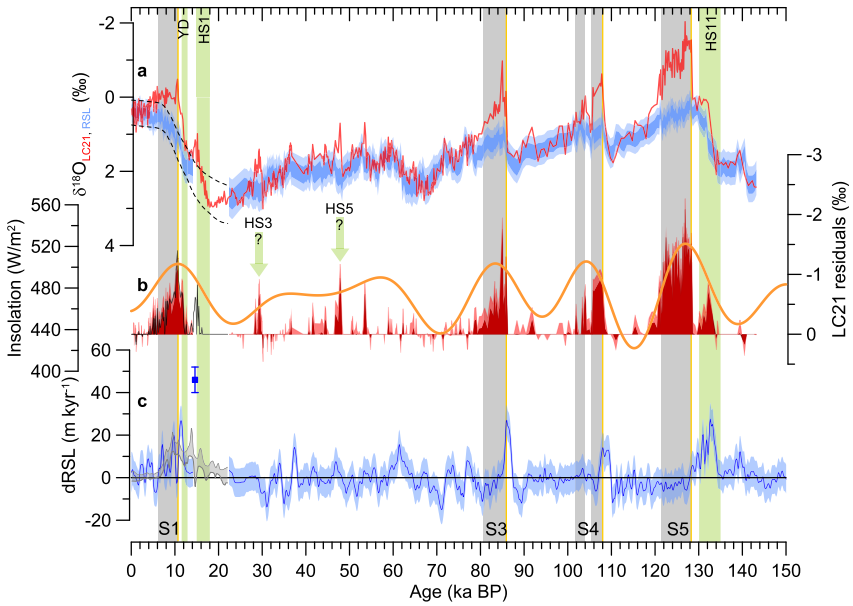

Fig. 3. **a**) Planktonic foraminiferal (*G. ruber*) $\delta^{18}O$ record from core LC21 (red), superimposed on a maximum probability sea-level record (Grant et al., 2012, 2014, based on the Red Sea sea-level reconstruction method of Siddall et al., 2003, 2004 and Rohling et al., 2009) which has been converted into equivalent Mediterranean $\delta^{18}O$ values following Rohling et al. (2014) (darker blue shading = 68% confidence limits; lighter blue shading = 95% confidence limits). The RSL record is unreliable ca 14–23 ka BP so the probabilistic sea-level reconstruction of Stanford et al. (2011), (which is based on radiometrically dated sea-level indicators), has also been converted into equivalent Mediterranean $\delta^{18}O$ values (black dashed lines = 2σ error). **b**) LC21 $\delta^{18}O$ 'residuals' beyond the 68% (pale red) and 95% (dark red) confidence limits of the Red Sea sea-level equivalent $\delta^{18}O$ variations, and beyond the 95% (black line) confidence limits of the Stanford et al. (2011) sea-level equivalent $\delta^{18}O$ variations. A potential correlation between negative residuals and Heinrich Stadials (HS) 3 and 5 is based on the timing of Dansgaard-Oeschger stadials in Greenland ice (Rasmussen et al., 2014). Boreal summer insolation at 65°N (orange; after Laskar, 1990) is also shown. **c**) Maximum probability record of rates of sea-level change (dRSL) with its 95% probability interval (blue envelope; equivalent to 2σ) (Grant et al., 2012, 2014), based on the Red Sea sea-level reconstruction method (Siddall et al., 2003, 2004; Rohling et al., 2009). The record is unreliable ca 14–23 ka BP so meltwater pulse 1A (Deschamps et al., 2012) is also indicated (blue square with 2σ error bars), as well as Stanford et al.'s (2011) record of sea-level change rates (grey shading = 95% probability interval). The timing of sapropels S1-S5 (grey rectangles), the Younger Dryas (Rasmussen et al., 2014) and Heinrich Stadials 1 (Álvares-Solas et al., 2011) and 11 (Marino et al., 2015) (green rectangles), and an inferred sharp increase in monsoon run-off into the eastern Mediterranean (yellow lines) are also indicated.

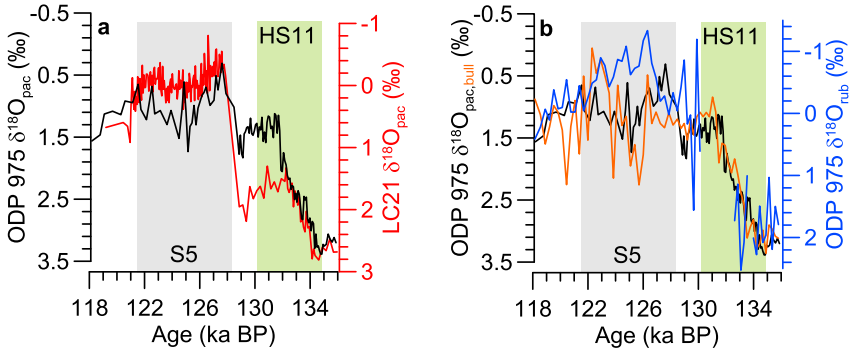

Fig. 4. Stable oxygen isotope records through sapropel S5 of **a**) *N. pachyderma* from core LC21 (red) and ODP Site 975 (black; Marino et al., 2015), on the radiometrically constrained chronology of Grant et al. (2012), and **b**) *N. pachyderma* (black; Marino et al., 2015), *Globigerinoides bulloides* (orange), and *G. ruber* (blue) (Kandiano et al., 2014) from ODP Site 975. The timing of Heinrich Stadial 11 (Marino et al., 2015) is also indicated (green rectangle).

available for the penultimate deglaciation. The negative LC21 residuals spike ca 133 ka occurs ~1–2 ky after the onset of termination 2 (i.e., closer to the onset of deglaciation than during termination 1), so alpine meltwater may have contributed to this isotopic depletion in LC21. However, the relatively small volume and ^{18}O depletion of alpine meltwaters compared to global ice sheets means that North Atlantic meltwaters propagating into the eastern Mediterranean would likely dominate any $\delta^{18}O$ meltwater signals in LC21. Further data are needed to address this question.

Regarding meltwater from European ice sheets, recent work suggests that drainage of the EIS at the end of the last glacial cycle was predominantly into the North Atlantic (Toucanne et al., 2015a), but there is also evidence that meltwater from the Fennoscandian ice sheet (FIS) flowed into the Black Sea during HS1, and that this overflowed into the northern Aegean Sea (Soulet et al., 2013). Other studies of Black Sea sediments, however, suggest generally stable environmental and hydrologic conditions through the last deglaciation until 14.5 ka BP, despite an interruption between 16.5 and 14.8 ka BP which was linked to input of sediments from a northern source (possibly the FIS) (Major et al., 2006; Bahr et al., 2006, 2008). Those and other studies (Sperling et al., 2003; Rohling et al., 2015) agree that reconnection of the Black Sea with the Mediterranean

appears to have been established much later, ca 9 ka BP. There are far fewer robust observations for the penultimate deglaciation, so in view of available evidence, we surmise that any input of meltwater from European ice sheets directly into the Mediterranean was likely relatively small for the last deglaciation, and therefore would not significantly affect the LC21 $\delta^{18}O$ residuals.

In short, the timing, volume and isotopic composition of alpine run-off into the Mediterranean over glacial-interglacial timeframes is not well constrained. While this freshwater source cannot be ruled out, the close timing between negative spikes in the LC21 residuals, ^{18}O depletions in the western Mediterranean, and HS suggests that the propagation of meltwater from the North Atlantic into the eastern Mediterranean explains most of the negative LC21 residuals at the end of HS1 and within HS11 (Fig. 3b). This is the first time such an inference has been made for the eastern Mediterranean, and it has important new implications for the interpretation of eastern Mediterranean $\delta^{18}O$ records, including those from speleothems whose source waters derive from eastern Mediterranean sea-surface water.

3.3. Local climatic effects

Next we consider local climatic influences on Mediterranean surface-water $\delta^{18}O$, and how these may manifest in the LC21 residuals. Such influences include sea surface temperature (SST), regional precipitation/evaporation, and African monsoon run-off.

3.3.1. Temperature

The RSL-to-$\delta^{18}O$ conversion accounts for glacial-interglacial Mediterranean SST contrasts of +5 °C (summer) and +3.5 °C (winter), with probabilistically determined uncertainties (see Rohling et al., 2014). These gradients are based on reconstructions for the LGM-to-Present (Hayes et al., 2005) and agree with isotope- and alkenone-derived SST estimates (Cita et al., 1977; Emeis et al., 2003). Such reconstructions also imply, however, that the penultimate glacial-interglacial SST gradient in the eastern Mediterranean was up to double that of the LGM-to-Present (Cita et al., 1977; Emeis et al., 2003). In that case, the sharp rise in negative LC21 residuals at the onset of sapropel S5 (Fig. 3b) might partly reflect a SST increase that has not been accounted for in the RSL-to-$\delta^{18}O$ conversion.

We have converted existing SST data for core LC21 (Marino et al., 2007, 2009) to our U/Th-related chronology (Fig. 5a,b). Although the data only cover the intervals of sapropels S1 and S5, detailed SST reconstructions for the eastern Mediterranean (Emeis et al., 2000, 2003) suggest that glacial-interglacial SST increases were greater immediately prior to S1 and S5 than for S3 and S4. Hence, any temperature effects on the LC21 residuals at the onset of S3 and S4 should be less pronounced than those for S1 and S5. The RSL-to-$\delta^{18}O$ conversion used to calculate the LC21 residuals (Section 3.1) is based on LGM-to-Present temperature gradients; therefore, the residuals record implicitly takes into account any SST increases prior to the onset of sapropels S1, S3 and S4. 'Small-scale' temperature variations are not accounted for in the RSL-to-$\delta^{18}O$ conversion, although their effect on the LC21 residuals at sapropel onset would likely be negligible compared to the larger warming trends. Regarding sapropel S5, the LC21 (Fig. 5b) and comparable SST records (e.g., for southern Aegean core MD40/67 in Emeis et al., 2003) suggest a glacial-interglacial temperature gradient that was 3–4 °C (equivalent to a maximum of 0.8‰) greater than that of the last deglaciation. Allowing for this ~1‰ change due to SST changes means that at least 0.5‰ of the negative shift in residuals at the onset of S5 must still be explained.

3.3.2. Precipitation–evaporation

Any temperature effects on foraminiferal calcite $\delta^{18}O$ would be (partly) offset by fractionation effects on seawater $\delta^{18}O$ due to evaporation. Hence, our inferred depletions in LC21 residuals due to increased SSTs should be viewed as maximum estimates, and were likely lower. The next question is therefore: to what extent do the remaining negative residuals (Fig. 3b) reflect a decrease in net evaporation from the Mediterranean region during times of sapropel deposition? This has long been debated, reflecting the contrasting and/or so far ambiguous proxy evidence (mainly pollen data) for hydrological changes in the eastern Mediterranean region at times of sapropel formation (see Tzedakis, 2007, 2009 and Rohling et al., 2015 for overviews).

For example, Kallel et al. (1997, 2000) inferred that the salinity of eastern Mediterranean surface waters (SSS) was homogenous during sapropel deposition, and suggested that this reflected an increase in local precipitation. However, a statistical assessment of $\delta^{18}O$ gradients through the Mediterranean basin for the time of S1 deposition indicated that strongest depletion clearly occurred in the Levantine region, in the vicinity of the Nile outlet (Rohling and De Rijk, 1999). Those authors also contested the calibration of $\delta^{18}O$ into SSS as used by Kallel et al. (1997, 2000), because the modern sea-surface salinity:$\delta^{18}O$ ratio in the Mediterranean does not hold for periods of enhanced freshwater input to the basin; that objection was further quantified by Rohling (1999) and Rohling et al. (2004). The importance of 'other freshwater sources' (than the Nile) to the eastern Mediterranean at the beginning and end of sapropel S5 deposition was also suggested by Scrivner et al. (2004), based on an apparent disparity between trends in Nd isotopes and residual $\delta^{18}O$ (i.e., corrected for temperature and ice-volume effects) across S5 at ODP site 967. However, the Nd record is of lower resolution compared to the $\delta^{18}O$ residuals, and, even if the offset is real, run-off from the wider North African margin could account for 'other freshwater sources', as was shown by Osborne et al. (2008). Palynological studies of the eastern Mediterranean have also inferred an increase in summer precipitation during times of sapropel formation (e.g., Rossignol-Strick, 1987, 1999; Wijmstra et al., 1990; Rossignol-Strick and Paterne, 1999; Langgut et al., 2011). However, Tzedakis (2009) questioned the reliability of these interpretations, and suggested that drought-resistant species or winter precipitation equivalent to the present-day regime could explain the observed trends, without the need to invoke enhanced summer precipitation. This interpretation is supported by Toucanne et al. (2015b), who inferred an increase in winter precipitation over the northern Mediterranean borderlands (NMB) during warm intervals of interglacials over the past 547 kyr, based on a suite of geochemical and lithological tracers of Golo River run-off into the northern Tyrrhenian Sea (core GDEC-4-2, Fig. 1).

In contrast, a comprehensive review of evidence for humidity changes in the Levant over the last two glacial-interglacial cycles concluded that, in general, it was the glacial (rather than interglacial) periods that were wetter (Frumkin et al., 2011). This is quantitatively supported by calculations of Dead Sea (=Lake Lisan) levels over the past 120 ka BP (Rohling, 2013). Similarly, groundwater isotope data suggest that Saharan aquifers were recharged during glacial rather than interglacial periods (Abouelmagd et al., 2012, 2014). However, speleothem growth periods in the Negev Desert (Israel) – indicative of wetter intervals – generally coincide with interglacials and monsoon maxima/precession minima (i.e., sapropel intervals), but not always: the Northern Negev appears to have been arid at 105 ka (≈sapropel S4) and 11 ka (≈S1) (Vaks et al., 2006).

Despite these apparently disparate findings, a consensus is emerging that they can be explained by increased seasonality and winter precipitation in the eastern Mediterranean during

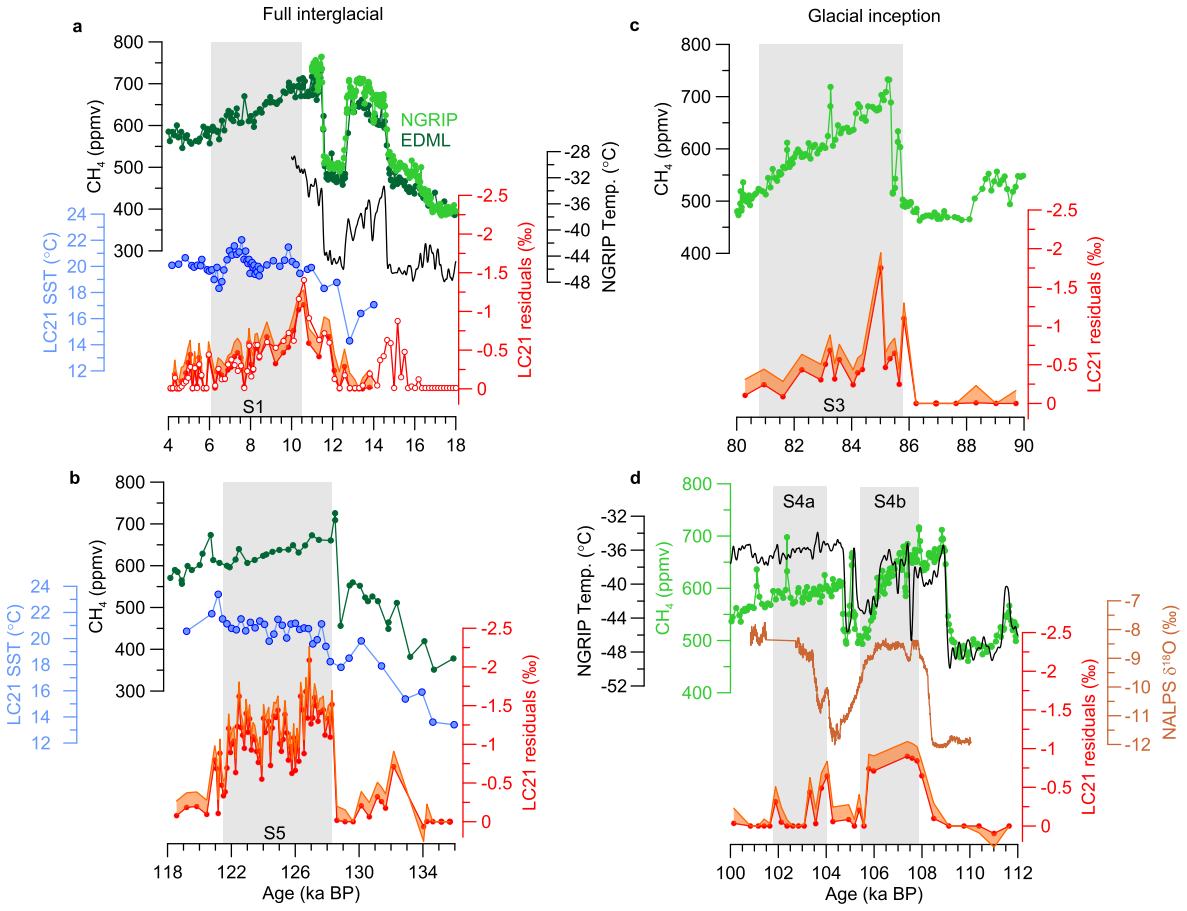

Fig. 5. Ice-core methane (CH_4) variations from Greenland (NGRIP; Baumgartner et al., 2014) (**a**, **c**, **d**) and from Antarctica (EDML; Schilt et al., 2010) on the AICC2012 chronology (Bazin et al., 2013) (**b**), compared with LC21 residuals beyond the 68% (orange) and 95% (red) confidence limits of sea-level equivalent $\delta^{18}O$ variations. In (**a**), LC21 residuals are also calculated using the Stanford et al. (2011) sea-level reconstruction (open red circles) (see Fig. 3). The NGRIP temperature record is also in **a** and **d** (black; Kindler et al., 2014) and a U/Th-dated speleothem $\delta^{18}O$ record (brown) from the northern European Alps (NALPS; Boch et al., 2011) is shown in **d**. Intervals shown are for full interglacial conditions (**a**, **b**) and periods of glacial inceptions (**c**, **d**). Previously published sea surface temperature (SST) records from LC21 (blue) were derived from alkenones (**b**; Marino et al., 2007) and from planktonic foraminiferal data (**a**; Marino et al., 2009), and have been converted to the Grant et al. (2012) chronology used here.

precession minima (Tzedakis, 2007; Frumkin et al., 2011; Milner et al., 2012; Rohling et al., 2015; Toucanne et al., 2015b). This argument is supported by recent simulations using a high-resolution, fully coupled ocean-atmosphere general circulation model (Bosmans et al., 2015). If we assume the 'winter precipitation' hypothesis to be correct, the key question then is what would be the effect of increased winter rainfall on eastern Mediterranean sea-surface $\delta^{18}O$, and could that explain negative LC21 $\delta^{18}O$ residuals during precession minima? In Bosmans et al.'s (2015) simulations, the predicted winter precipitation was not uniform over the Mediterranean but focussed over the Ionian and Levantine Seas, and was associated with local convection rather than eastward propagating storm tracks from the North Atlantic. Interestingly, no increase in either summer or winter rainfall over the NMB during precession minima was indicated, whereas both summer and winter rainfall increased over the Levant. These observations suggest that the effect on surface water $\delta^{18}O$ of any precipitation increase would be localised; furthermore, this effect would likely be either negligible (i.e., balanced by increased evaporation from the same basin) or an increase in $\delta^{18}O$ values (if locally evaporated moisture precipitated outside the catchments of the eastern Mediterranean basin) (Rohling et al., 2015).

To further investigate these effects, we developed a record of 'Soreq excess $\delta^{18}O$' ($\delta^{18}O_{SOREQ\ XS}$) for the Soreq cave (Israel) speleothem $\delta^{18}O$ record ($\delta^{18}O_{speleo}$) by subtracting the LC21 $\delta^{18}O_{ruber}$ record from it (Fig. 6). The $\delta^{18}O_{SOREQ\ XS}$ record thus represents a deconvolved local eastern Mediterranean climate signal, from which any bias related to monsoon/riverine run-off or global glacial cycles has been removed. This calculation is possible because *i)* there is a direct evaporation-precipitation link between the $\delta^{18}O$ composition of eastern Mediterranean surface waters and speleothems from the Levant (Matthews et al., 2000; Bar-Matthews et al., 2003; McGarry et al., 2004; Kolodny et al., 2005; Almogi-Labin et al., 2009; Marino et al., 2009; Grant et al., 2012), *ii)* temperature variations in eastern Mediterranean surface waters and Soreq cave are coupled (Bar-Matthews et al., 2003; Affek et al., 2008), and *iii)* the $\delta^{18}O_{speleo}$ and $\delta^{18}O_{ruber}$ records have been previously synchronised (Grant et al., 2012). We first interpolated the $\delta^{18}O_{speleo}$ and $\delta^{18}O_{ruber}$ records to the same age-steps, subtracted the mean from each record so that they were centred about a mean of zero, and then subtracted the zero-centralised $\delta^{18}O_{ruber}$ from the zero-centralised $\delta^{18}O_{speleo}$. The uncertainty of $\delta^{18}O_{SOREQ\ XS}$ about the mean value (±0.38 at 2σ) was calculated using a root mean squares calculation, and combines uncertainties for the average Late Holocene value of $\delta^{18}O_{speleo}$ (±0.29) and $\delta^{18}O_{ruber}$ (±0.24).

The $\delta^{18}O_{SOREQ\ XS}$ values suggest that most of the S1, S3, and S4 intervals were not characterised by systematically wetter/warmer conditions in the Levant (Fig. 6b), although an inferred decrease in net evaporation during brief (<1 ky) periods within the latter halves of sapropels S1 and S4 can account for some of the variability

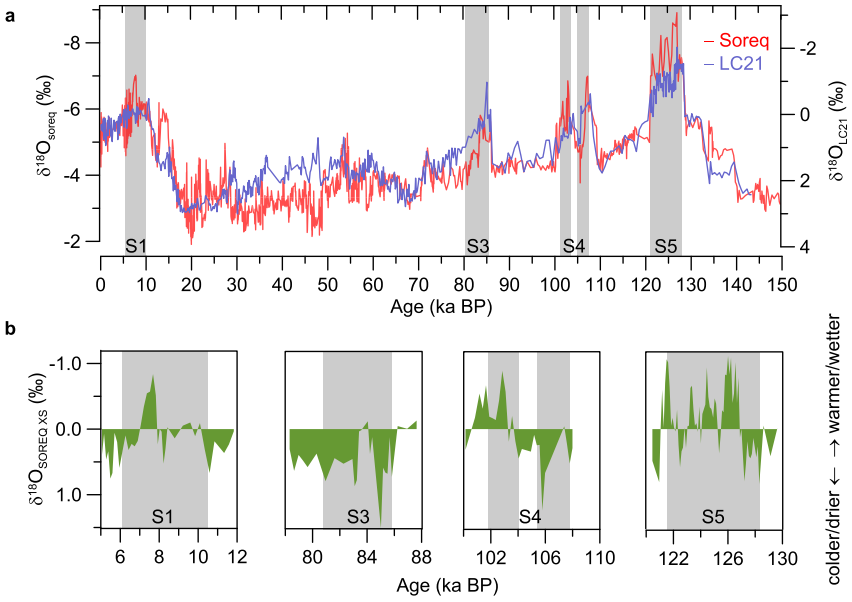

Fig. 6. **a**) Soreq cave speleothem $\delta^{18}O$ (red; Grant et al., 2012) and LC21 *G. ruber* $\delta^{18}O$ (blue). **b**) Soreq cave 'excess' $\delta^{18}O$ ($\delta^{18}O_{SOREQ\ XS}$) after removal of source-water $\delta^{18}O$ signal (green; see Section 3.3.2) for sapropels S1, S3, S4 and S5 (grey rectangles).

in the residuals at those times. In contrast, $\delta^{18}O_{SOREQ\ XS}$ implies intermittently wetter/warmer conditions at Soreq Cave during sapropel S5 (Fig. 6b). These interpretations are broadly consistent with the findings of Vaks et al. (2006), who noted that not all monsoon maxima/precession minima were associated with more humid intervals in the Levant. Specifically, both $\delta^{18}O_{SOREQ\ XS}$ and the Vaks et al. (2006) study imply that the interval of S5 was generally more humid, while the S4 and S1 intervals were relatively arid. The $\delta^{18}O_{SOREQ\ XS}$ record suggests that the S3 interval was also relatively arid, although the Vaks et al. (2006) study suggests that this interval was more humid. We note that the Bosmans et al. (2015) 'precession minima' simulations were performed for maximum eccentricity only, i.e., equivalent to the orbital configuration for S5; future modelling of precession minima of different intensities is therefore needed to fully validate the observational data. Finally, positive $\delta^{18}O_{SOREQ\ XS}$ values in the earliest part of S5 imply drier conditions in the eastern Mediterranean at that time. This is consistent with evidence for a peak in Mediterranean sclerophylls during the initial period (first ~2 kyr) of interglacials, which strongly suggests summer aridity (Tzedakis et al., 2002, 2003; Tzedakis, 2009, and references therein). Hence, the sharp decrease in LC21 residuals at the onset of S5 (Fig. 3b) is not likely to represent decreased net evaporation in the eastern Mediterranean region.

To sum up, minimal climatic influences can be attributed to the LC21 residuals through S1, S3 and S4, and a maximum of −1‰ (likely less) of the LC21 residuals through sapropel S5 can be explained by local climate changes. We therefore conclude that most of the abrupt negative shifts in LC21 residuals at the onset of sapropels are unlikely to be due to local climatic changes, and instead reflect external, monsoon-related run-off into the eastern Mediterranean from the Nile and wider North African margin (e.g., Rossignol-Strick, 1985; Rohling, 1999; Rohling et al., 2002; Scrivner et al., 2004; Osborne et al., 2008, 2010).

4. A proxy for African monsoon run-off

A useful means for validating our conclusion that the LC21 residuals predominantly reflect African monsoon run-off into the eastern Mediterranean, is to compare them with past changes in atmospheric methane (CH_4) concentrations. Such changes are closely related to the extent of tropical wetlands, and therefore also to changes in monsoon precipitation (Chappellaz et al., 1990; Spahni et al., 2011). Alternatively, we could compare the residuals to other African monsoon proxy records, yet this is not straightforward due to *i)* large spatial and temporal heterogeneity in African monsoon precipitation, *ii)* variable threshold responses among different precipitation/monsoon proxies, *iii)* a dearth of suitable records extending from the Holocene to MIS 5e, and *iv)* chronological uncertainties within and between different proxy records (see Gasse, 2000). While ice-core CH_4 records are not without chronological uncertainties, and do not unambiguously reflect monsoon variability (for instance, they are also coupled to northern hemisphere temperature fluctuations; see Baumgartner et al., 2014), they are advantageous because they provide a continuous, high resolution, well-mixed (spatially and temporally) signal over the entire last glacial cycle that is strongly coupled to boreal tropical hydrological changes. We therefore compare our LC21 residuals with ice-core CH_4 records from Greenland (North Greenland Ice-core Project (NGRIP); Baumgartner et al., 2014) and from Antarctica (EPICA Dronning Maud Land (EDML); Schilt et al., 2010; Bazin et al., 2013) (Fig. 5). Fig. 5 reveals good agreement in the timing of abrupt CH_4 increases and negative LC21 residuals prior to sapropel onset, for all four sapropel intervals considered here.

The agreement is excellent for S3 and S5 at sapropel onset (Fig. 5b,c). A smaller peak in the LC21 residuals before S5 (ca 132 ka) can be (partly) explained by isotopically light meltwater reaching the eastern Mediterranean (Section 3.2), so we do not compare the LC21 residuals and CH_4 over this interval. For S4, methane levels start to increase ~0.5–1 kyr before the LC21 residuals decrease (Fig. 5d). While this offset is within the age uncertainties of both records, the timing of the LC21 residuals decrease is very closely aligned with a marked increase in $\delta^{18}O$ in a U/Th-dated speleothem ('NALPS'; Boch et al., 2011) from the European Alps (Fig. 5d). The NALPS record primarily reflects high-latitude temperature variations in the wider North Atlantic, and is remarkably similar to NGRIP temperature reconstructions (Boch et al., 2011). Given that

NGRIP methane and temperature records are directly in phase over the last glacial cycle (Baumgartner et al., 2014) (Fig. 5d), the U/Th-dated NALPS record can be used to independently validate the NGRIP chronology in this interval. In detail, this reveals a clear offset between shifts in the NALPS and NGRIP records prior to the onset of sapropel S4 and within the S4 interruption (Fig. 5d), which suggests that the NGRIP chronology may be ~1 ky too old at around 108 ka BP. Interestingly, our U/Th-based chronology for the LC21 residuals yields a much closer agreement to the U/Th-dated NALPs record than to the NGRIP methane and temperature records (Fig. 5d). Thus, the CH_4 and LC21 residuals records may be more closely in phase than Fig. 5d suggests, once the apparent age correction is implemented to the NGRIP records.

For sapropel S1, the timing of two abrupt CH_4 rises appears to be slightly offset from decreases in the LC21 residuals (Fig. 5a). This offset may simply reflect age model uncertainties (in LC21 and/or the ice cores), yet this is arguably the most reliably dated section of all cores. An alternative explanation is that negative peaks in LC21 residuals at 15.5–14.3 ka BP, 12.5 ka BP, and at 11.8–11.6 ka BP may (partly) relate to meltwater release into the North Atlantic during the last deglaciation. As explained in Section 3.2, such meltwater pulses would bring isotopically light $\delta^{18}O$ into the Mediterranean, and this has not been accounted for in the RSL-to-$\delta^{18}O$ conversion which is used to calculate the LC21 residuals. A third explanation is that northern hemisphere temperature, rather than tropical precipitation, accounts for most of the CH_4 signal at this time. Both the NGRIP temperature and CH_4 records clearly show the Bølling-Allerød warm interval (~13–15 ka BP), which is less apparent in the LC21 residuals (Fig. 5a). Given these various explanations, we do not attempt to interpret the LC21 residuals outside of the peak monsoon run-off interval associated with sapropel S1. In that case, there is generally good agreement between the LC21 residuals and CH_4 records from ~11 ka BP onwards (Fig. 5a). Thus, considering all four sapropels in LC21, the CH_4 records support our inference that the LC21 residuals reliably track African monsoon run-off into the eastern Mediterranean at times of sapropel deposition.

5. Discussion

5.1. Monsoon–sapropel phasing

Our reconstructions suggest that the increases in African monsoon run-off associated with sapropels S3, S4 and S5 are sharply delineated, and coincide closely with the starts of sapropel deposition. For sapropel S1, the onset of the monsoon signal seems somewhat masked in the LC21 residuals, likely due to meltwater effects (Fig. 3; Section 3.2). Nonetheless, an abrupt increase in monsoon run-off to peak values coincides with the onset of S1. These coherent observations suggest that monsoon-related freshwater inputs to the eastern Mediterranean were a primary driver in triggering the onset of sapropel formation, consistent with conventional views (e.g., Rossignol-Strick, 1985; Emeis et al., 1996; Ziegler et al., 2010a).

The timing of sapropels (and monsoonal flooding) relative to insolation/precession, however, varies by up to ~3 kyr, irrespective of whether the sapropel onset or mid-point is used for phase calculations (Table 2, Fig. 7). We focus on sapropel mid-point phasings in order to compare our results with previous studies (Lourens et al., 1996, 2004; Ziegler et al., 2010a). The mid-points of sapropels S3 and S4 in core LC21 occurred within 0.1–0.8 kyr of precession minima and insolation maxima (Table 2; Fig. 7c,d), whereas the mid-points of sapropels S1 and S5 lag the nearest precession minimum/insolation maximum by 2.1–3.3 kyr (Table 2; Fig. 7a,b). Previous studies inferred a lag of ~3 kyr between the mid-point of S1 and the nearest precession minimum/insolation maximum (Lourens et al., 1996, 2004; Ziegler et al., 2010a), and we find a comparable phase offset for S1. We find that it also appears to be valid for S5, but not for S3 or S4. We note, however, that the mid-point ages for S1, S3, S4 and S5 in Ziegler et al. (2010a) are all within chronological uncertainties of the new mid-point ages presented here, when we consider what Ziegler et al. (2010a) termed “precursory events” of S3 and S4 as part of the sapropel.

It is worth bearing in mind that the timing of a sapropel mid-point depends on the duration of sapropel deposition, as noted by Emeis et al. (2003), and this clearly varies (Table 1). In core LC21, the largest discrepancy between sapropel durations is between S1 and S5 (2.4 kyr, Table 1), yet both sapropels exhibit a similar precession-lag. Furthermore, S4 and S5 have similar durations, yet very different insolation phasings (Tables 1 and 2). Therefore, differences among sapropel mid-point phasings with respect to precession are not simply an artefact of variable sapropel deposition periods. An alternative approach is to consider sapropel–insolation phasings based on the onset rather than mid-point of a sapropel. This makes sense because African monsoon precipitation is influenced by positive vegetation-albedo feedbacks which vary with insolation intensity (Nicholson, 2009). These feedbacks are therefore unlikely to be the same for all sapropels. However, at the onset of elevated monsoon run-off (= sapropel deposition), such feedbacks would not yet have had time to fully develop. Hence, the timing of sapropel onsets should be less biased by feedback processes than the timing of sapropel mid-points. As noted above, in LC21 we observe similar (relative) differences among sapropel–insolation phasings using the onset and mid-point criteria (Table 2), which suggests that our inferred phase relationships are robust.

Regardless of possible explanations for the above phase differences, our observations suggest that *1)* the concept of a consistent 3-kyr lag between precession minima/insolation maxima and an interval of sapropel deposition is valid only within broad uncertainties of a few thousand years, and *2)* insolation is not the sole driver of African monsoon dynamics, given that insolation–monsoon phasings do not seem to be consistent among the sapropels considered here.

5.2. Sea level–sapropel phasing

In core LC21, the deposition of sapropels S3, S4 and S5 began after sea level had risen to a relative ‘highstand’, despite differences in the height of these highstands (Fig. 7b–d). Conversely, sapropel S1 was deposited when sea level was still rising, and its onset occurred ~4 kyr before a highstand (Fig. 7a). These observations suggest that the relative timing of the Holocene sapropel (S1) was unique for the last glacial cycle. However, when considering rates (dRSL) and amplitudes of sea-level change, rather than RSL itself, we see another pattern, namely a clear discrepancy between sea level–sapropel phasings between early interglacial and glacial-inception periods (Fig. 7). In the interglacial case (S1 and S5), sapropel deposition began after sea-levels had risen ~90 m, and after a 50–75% reduction in rates of sea-level rise from their peak rates (Fig. 7a,b). In the case of glacial inception times (S3 and S4), the onset of sapropel deposition occurred after substantially smaller sea-level rises (~15–35 m), and just after sea-level rise rates peaked (Fig. 7c,d).

These results imply that over the last glacial cycle, sapropel deposition was sensitive to sea-level changes, in agreement with Grimm et al.'s (2015) model experiments for sapropel S1. In those experiments, monsoon forcing alone could not explain S1 formation because the development of deep-water anoxia took several millennia, i.e., longer than the timespan between monsoon onset and S1 deposition. However, Grimm et al.'s (2015) simulations also

Table 2
Lag between sapropel mid-points/onset and maxima in June-July insolation at 65°N ($INSOL_{MAX}$), maxima in the summer inter-tropical insolation gradient ($SITIG_{MAX}$), and precession minima (P_{MIN}). Negative values mean that sapropel mid-points/onset lead the equivalent insolation maxima/precession minima. Red text denotes phase offsets >2 kyr.

Phase:	Insolation:$Sapropel_{MID}$			Insolation:$Sapropel_{ONSET}$		
(kyr)	($INSOL_{MAX}$)	($SITIG_{MAX}$)	(P_{MIN})	($INSOL_{MAX}$)	($SITIG_{MAX}$)	(P_{MIN})
S1	2.5	2.8	3.3	0.3	0.6	1.1
S3	0.1	0.8	-0.3	-2.4	-1.7	-2.8
S4	-0.5	-0.2	0.7	-3.6	-3.2	-2.3
S5	2.1	2.6	2.1	-1.3	-0.8	-1.3

showed that monsoon forcing nonetheless contributed to S1 deposition because the additional freshwater inputs led to strong changes in density gradients; these in turn affected the vertical extent and duration of S1 anoxia. We observe close timing relationships for both sea-level and monsoon changes among all sapropels considered here, which occurred under a wide range of insolation and ice-volume forcings. We also observe that the relationships with sea-level change are not straightforward, and that different interpretations arise depending on comparison with sea-level itself, or with rates of sea-level change (see below).

5.3. Sapropel formation: sea-level versus monsoon control

Our data strongly suggest that the onset of sapropel deposition

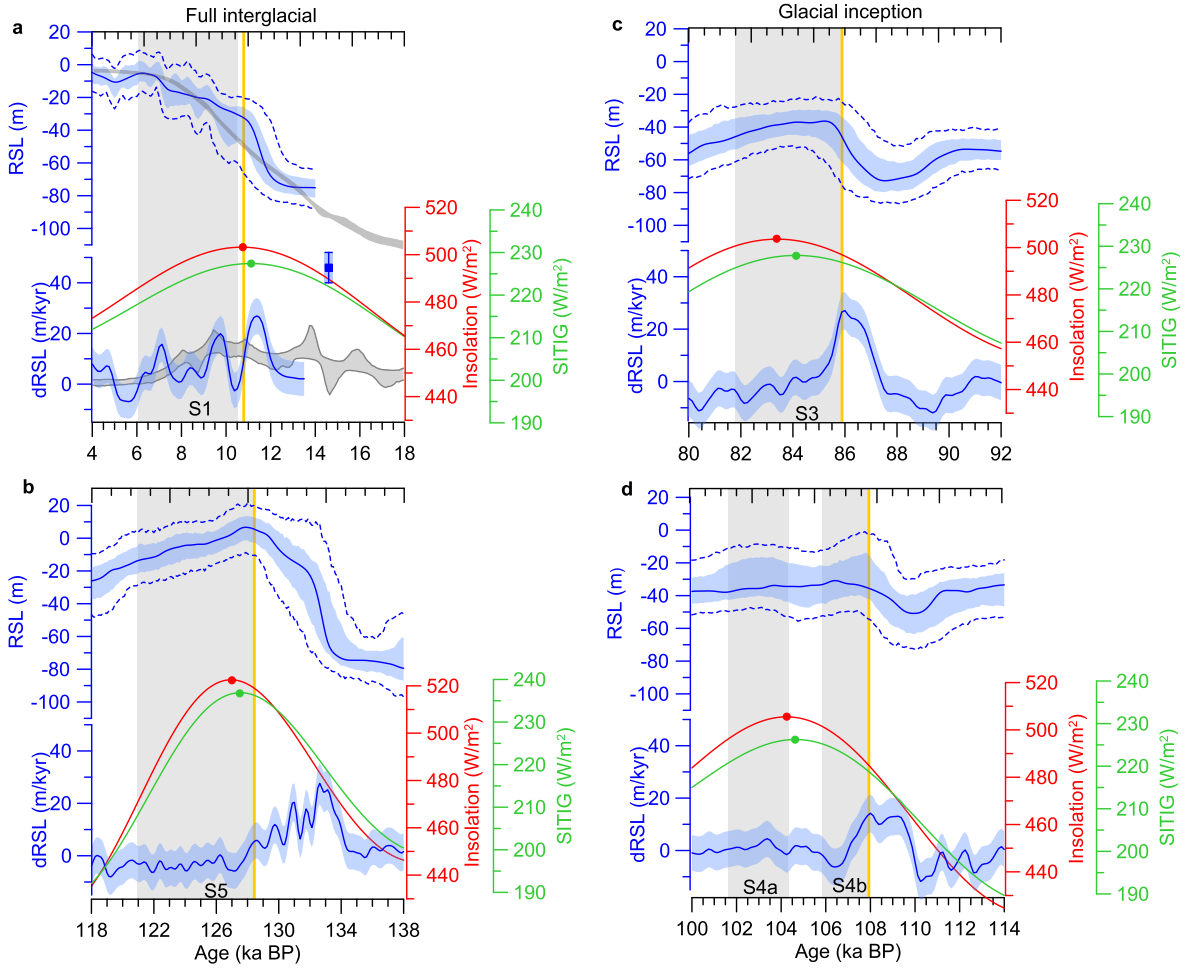

Fig. 7. Ice-volume and insolation changes spanning sapropel intervals under full interglacial conditions (**a**, **b**) and periods of glacial inceptions (**c**, **d**). Maximum probability curves of relative sea-level (RSL, blue) and its rates of change (dRSL, black) with their 95% probability intervals (paler envelopes; equivalent to 2σ) (Grant et al., 2012, 2014) are based on the Red Sea sea-level reconstruction method (Siddall et al., 2003, 2004; Rohling et al., 2009). The 95% confidence intervals for all RSL data (blue dashed lines) are also shown. The Red Sea RSL and dRSL data are unreliable ca 14–23 ka BP so in (**a**) we also show Stanford et al.'s (2011) 95% probability intervals of sea level and sea-level change rates (grey shading), as well as meltwater pulse 1A (Deschamps et al., 2012). Insolation curves are for boreal summer at 65°N (red) and the summer inter-tropical insolation gradient (SITIG; green) (based on Laskar, 1990), with filled circles indicating maxima. Sapropels (grey rectangles) and an inferred sharp increase in monsoon run-off into the eastern Mediterranean (yellow lines) are also indicated.

over the last glacial cycle was sensitive to both sea-level change and monsoonal flooding of the eastern Mediterranean. While increased freshwater input to the Mediterranean from the northern Mediterranean Borderlands (NMB) has frequently been proposed to have also contributed to sapropel formation (Section 3.3.2), and cannot be entirely ruled out, the effect of this run-off on net buoyancy forcing has not yet been adequately quantified. Given that most precipitation over the wider eastern Mediterranean (including the NMB) is sourced from the basin itself, that implies little or no net effect on surface buoyancy changes (see Section 3.3.2). Hence, monsoon- and deglaciation-related changes in basin hydrography remain the most plausible mechanisms of surface buoyancy forcing at the time of sapropel deposition.

Given that our data show: *i)* synchronous onsets of sapropel deposition and monsoonal flooding into the eastern Mediterranean, and *ii)* variable sea-level (ice-volume) histories immediately prior to and at the onset of sapropel deposition among different sapropels, despite broad similarities among these histories, the most straightforward interpretation would be that the onset of sapropel deposition was closely related to monsoon forcing, and not so systematically controlled by deglaciation effects.

Nonetheless, especially for sapropel S1, a strong sea-level (and warming) influence may still exist (e.g., Grimm et al., 2015) because, out of the four sapropels considered here, S1 is the only one that was deposited immediately after a substantial sea-level rise, and sea level continued to rise throughout S1 deposition. A link between sapropel S1 formation and deglaciation was first demonstrated quantitatively by Rohling (1994) and Béthoux and Pierre (1999), who showed that the latter would lead to decreased surface- and intermediate-water salinities, which in turn would inhibit deep-water ventilation. This is because rising sea levels would have enhanced the exchange of Atlantic and Mediterranean waters at the Strait of Gibraltar by increasing the cross-sectional area of the strait (e.g., Bryden and Kinder, 1991; Rohling, 1999; Rogerson et al., 2012). The resultant decrease in residence time of Mediterranean waters, combined with the reduced salinity of inflowing Atlantic water due to melting ice sheets, would cause progressive surface buoyancy gain in the Mediterranean (Rohling et al., 2015). This relationship – between sea-level change and Mediterranean salinity – is well-defined and non-linear on glacial-interglacial timeframes (Rohling and Bryden, 1994) (as opposed to the modern stochastic relationship observed inter-annually by Pinardi et al. (2014)).

A relatively weak insolation maximum during the Holocene provides further support for the proposed role of sea-level rise in S1 deposition, because the monsoon maximum was probably less intense (de Noblet et al., 1996) than for other sapropels (namely S5; Rohling et al., 2004) and therefore may not have provided sufficient buoyancy forcing (via freshwater run-off) for deep-water stagnation. This argument is somewhat supported by the LC21 residuals through S1, in that they are roughly half the magnitude of those for S5 (Fig. 3), which was deposited during a relatively strong insolation maximum (Fig. 7b). Notwithstanding possible temperature effects on the LC21 residuals, our interpretation is further supported by a detailed study of stable isotopes ($\delta^{18}O$, $\delta^{13}C$) in multiple foraminiferal species through sapropels S1 and S5 in the eastern Mediterranean (Rohling et al., 2004). That study concluded that freshwater dilution of surface waters was much reduced during S1 compared to S5. Similarly, the duration of S1 is distinctly shorter (4.4 kyr) than that of S5 (6.8 kyr) (Table 1), which may be consistent with weaker monsoon-forcing of S1 compared to S5.

There is little differentiation among the LC21 residuals values for S1, S3 and S4 (Fig. 3b), or among the corresponding insolation values (Fig. 7), implying that sapropels S3 and S4 may have been

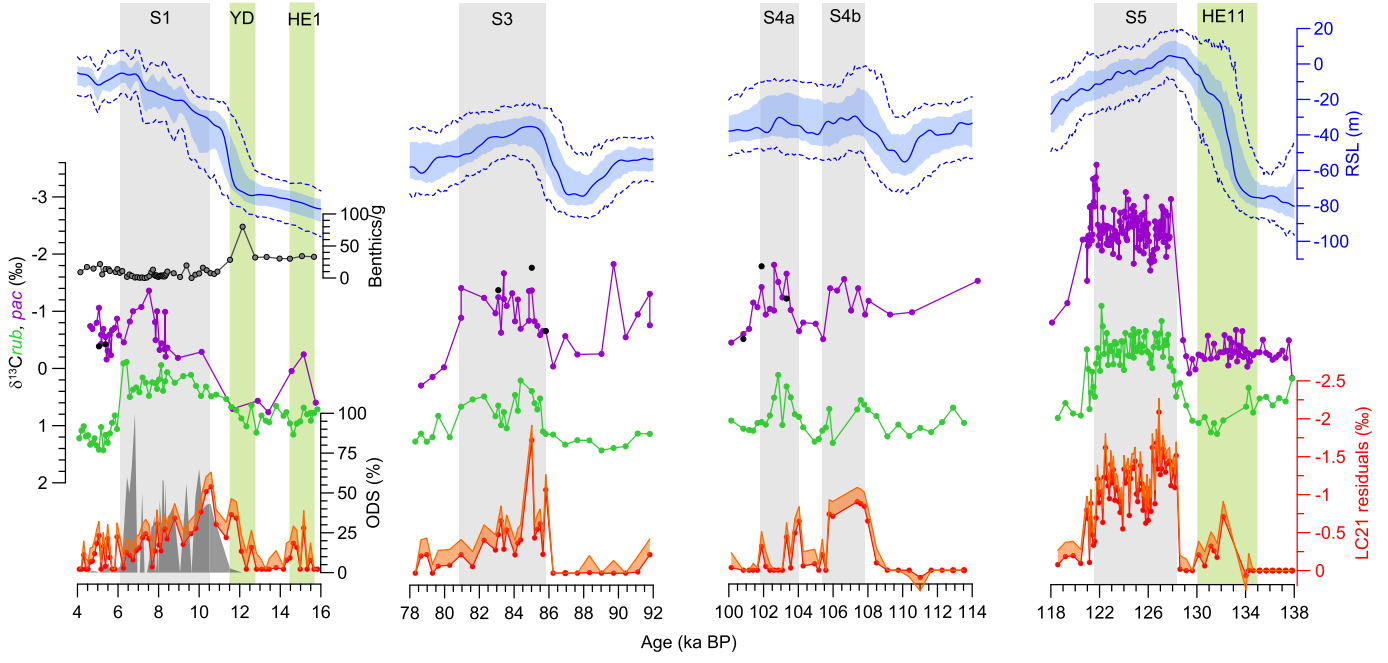

Fig. 8. Planktonic foraminiferal stable carbon isotope records from core LC21, for the surface-dwelling *G. ruber* ($\delta^{13}C_{ruber}$; green) and sub-surface dwelling *N. pachyderma* ($\delta^{13}C_{pac}$; purple) and *G. inflata* (panel **a** only; pink = normal test, blue = smooth test). Red Sea relative sea-level record (RSL; blue) and the Stanford et al. (2011) sea-level record (grey shading) as in Fig. 7. LC21 residuals (red with orange shading) as in Fig. 5). The timing of sapropels S1-S5 (grey rectangles) and of cold episodes in the North Atlantic (the Younder Dryas, YD (Rasmussen et al., 2014), and Heinrich Stadials 1 (Álvares-Solas et al., 2011) and 11(Marino et al., 2015) (green rectangles) are indicated. Previously published data from LC21 are also shown in panels **a** and **d**, after conversion to the Grant et al. (2012) chronology: Total number of benthic foraminifera (Benthics/g; grey line with dots) and percent oxygen deficient species (ODS, grey shading), from Abu-Zied et al. (2008) (panel **a**); weight percent organic carbon (C_{org}; brown shading), isorenieratene concentration (black line with dots), and percent *F. profunda* (pink), after Marino et al. (2007) and Grelaud et al. (2012) (panel **d**).

comparable to S1 in terms of relatively weak monsoon forcing. However, the durations of S3 and S4 exceed that of S1 (Table 1), and opposite sea-level trends are observed for S3 to S5 relative to S1: sea level either declined (by ~20 m during S3 and S5) or hovered around a broad plateau (S4) (Fig. 7). Furthermore, sea-level histories are noticeably different for the 5–6 kyr preceding S3 and S4 compared to S1 (this is the timeframe that Grimm et al. (2015) suggest to be crucial for a deglaciation influence on sapropel deposition). Falling sea level would have reduced the cross-sectional area of the Strait of Gibraltar and Strait of Sicily, leading to reduced Atlantic-Mediterranean exchange, longer Mediterranean residence times, and increased Mediterranean surface-water salinity in the more restricted and highly evaporative basin (e.g., Rohling, 1999; Rohling et al., 2014). The resultant increase in surface density would have promoted deep-water formation rather than stagnation. Although sea level was still rising at the very onset of S5, similar to S1, S5 deposition began 3–4 kyr after the main, rapid sea-level rise associated with termination II. It is hard to reconcile such timings with timescales for deep-water stagnation based on deglaciation effects alone (see below). For S3 and S4, sapropel onset coincides with peak rates of sea-level rise (Fig. 7c,d), which may imply some degree of sea-level control on the timing of sapropel onset, in addition to monsoon forcing.

To help clarify the processes leading to sapropel deposition, we can also consider general trends in the LC21 $\delta^{13}C$ records, together with previously published records from LC21 (Marino et al., 2007; Abu-Zied et al., 2008; Grelaud et al., 2012) which have now been converted to the radiometrically-based chronology used here (Fig. 8). We focus on sapropel onset and the prior 5–6 kyr because, as suggested by Grimm et al. (2015) for sapropel S1, at least 5.5 or 6 kyr (based on modelling and benthic $\delta^{13}C$ data, respectively) of progressive deep-water stagnation and oxygen consumption was required to initiate S1 deposition and anoxia. There is no consistent trend among the LC21 $\delta^{13}C$ profiles in the 5–6 kyrs preceding sapropel onset (Fig. 8), implying that the processes necessary for sapropel deposition (reduced ventilation, increased biological production) developed differently for each sapropel. The most notable disparity is between S1 and S3-S5. For S1, the $\delta^{13}C_{rub\text{-}pac}$ gradient is minimal for most of the pre-sapropel period, and both $\delta^{13}C_{rub}$ and $\delta^{13}C_{pac}$ start to decrease ~2–3 kyr before the S1 onset. This decline is mirrored in $\delta^{13}C$ values for *G. inflata* (Fig. 8), a planktonic foraminifer with a similar apparent ecological niche to *N. pachyderma*. In contrast, prior to S3-S5 there is a 1–2‰ gradient between $\delta^{13}C_{pac}$ and $\delta^{13}C_{rub}$, and a negative shift in both occurs much closer to sapropel onset, synchronous with a negative shift in the LC21 residuals. For S3 and S4, these shifts also coincide with rising sea levels, so without further proxy records it is difficult to conclusively distinguish between monsoon and deglaciation effects. However, the fact that $\delta^{13}C$ trends prior to S3 and S4 are arguably more similar to those pre-S5 than pre-S1, hints at a common development mechanism for S3, S4, and S5.

The most extensive datasets in LC21 are for S1 and S5 (Fig. 8). These two sapropels have already been studied extensively elsewhere (see Rohling et al., 2015, and references therein). However, the advantage of our study is that we can now unambiguously examine timing relationships between sea-level rise, monsoon run-off into the eastern Mediterranean, and key proxy records, on an independent and chronologically consistent age-scale (Fig. 8). Regarding S1, a spike in benthic foraminiferal abundances ('benthics/g') coincides with the YD (Fig. 8a); abundances then decline until the S1 onset. This decline coincides with rapidly rising sea levels, decreasing $\delta^{13}C$ values, and a sharp increase in oxygen deficient species (ODS) within the LC21 benthic foraminiferal assemblage (Abu-Zied et al., 2008; chronology after Grant et al., 2012) (Fig. 8a). Importantly, the rise to peak monsoon run-off occurs *after* the shift in benthic assemblages. This is compelling evidence for a key role of deglaciation in instigating vertical stratification and deep-water anoxia prior to S1 formation. At the same time, the synchronous onset of S1 and peak monsoon run-off into the eastern Mediterranean is equally strong evidence that S1 deposition was tied to monsoon forcing.

In contrast, benthic fossils in core LC21 disappeared at the onset of (rather than prior to) sapropel S5 (Marino et al., 2007). Similar observations for S5 have been made previously. For example, Schmiedl et al. (2003) studied a southeast Aegean core from a similar water depth to LC21, and observed relatively high benthic foraminiferal abundances right up until S5 onset. They concluded that bottom waters were sufficiently ventilated until the start of S5 deposition, despite an inferred stepwise reduction in oxygen content over the preceding ~3 kyr. Capotondi et al. (2006) also found a close agreement between the onset of benthic anoxia and S5 deposition, and Jorissen (1999) noted differences in benthic foraminifera assemblages between S1 and S5. In LC21, the onset of benthic azoic conditions during S5 coincides with abrupt increases in organic carbon (C_{org}) deposition, isorenieratene concentrations, and abundances of *Florisphaera profunda* coccoliths (Grelaud et al., 2012), as well as with negative peaks in the $\delta^{13}C$ and residuals records (Fig. 8d). The C_{org} increase is unlikely to be due solely to increased preservation, because the values are unusually high (up to 14%) for Aegean sediments (cf. typically 2–3%; Mercone et al., 2001; Thomson et al., 2004). Elevated isorenieratene concentrations are indicative of anaerobic phototrophic Chlorobiaceae, while increased abundances of *F. profunda* are associated with an increase in subsurface rather than surface primary productivity. Together, these records point to the rapid development of a deep chlorophyll maximum and euxinic conditions at the onset of S5 in LC21 (Marino et al., 2007; Grelaud et al., 2012). Thus, for S5, there is a strong timing relationship between substantial monsoon run-off into the eastern Mediterranean, benthic anoxia, increased (subsurface) productivity, and increased C_{org} deposition.

5.4. African monsoon variability

Our datasets, in line with previous studies based on less well constrained chronologies and/or fewer sapropel events (Rohling et al., 2002, 2004, 2006; Emeis et al., 2003; Marino et al., 2007; De Lange et al., 2008; Hennekam et al., 2014), strongly suggest that the timing of monsoon run-off into the eastern Mediterranean was crucial in triggering surface buoyancy changes necessary for sapropel deposition. Our results also show that the timing of this monsoon run-off, relative to insolation changes, varied over the last glacial cycle (Fig. 7). These timings were broadly similar for sapropels S1 and S5 (Fig. 7a,b) and for sapropels S3 and S4 (Fig. 7c,d). Comparable phasings were observed among sea level–sapropel relationships, whereby longer lags between insolation maxima and sapropel mid-points were observed for larger sea-level changes (Fig. 7; Table 2). These observations suggest that global ice-volume changes exceeding a certain magnitude interfere with the precession-pacing of the African monsoon.

An empirical link between African monsoon precipitation and glaciation has been inferred from model simulations. Freshwater hosing experiments for the North Atlantic suggest that the African monsoon weakened in response to (glacial) meltwater pulses (Chang et al., 2008; Tjallingii et al., 2008; Kageyama et al., 2013), due to atmosphere-ocean feedbacks associated with a reduced Atlantic meridional overturning circulation (AMOC) and a southward shift in the intertropical convergence zone (ITCZ) (Chang et al., 2008). Transient simulations (Otto-Bliesner et al., 2014) and a model set-up that included remnant ice sheets in addition to a North Atlantic freshwater influx (Lézine et al., 2011; Marzin et al.,

2013) show similar results to the previous hosing experiments. Notably, Lézine et al. (2011) and Marzin et al. (2013) concluded that a freshwater flux into the North Atlantic would have had a larger impact on African monsoon precipitation than the presence of remnant ice sheets alone. This is in line with our observations: the magnitude of sea level rise (and therefore meltwater effects), rather than sea level at sapropel onset, distinguish the more insolation-lagged sapropels S1 and S5 (Section 5.2; Fig. 7).

A link between past African monsoon variability and global ice-volume changes appears to be supported by proxy data. For example, precession-scale variability in a West African monsoon proxy record was interpreted in terms of large-scale changes in global ice volume (Weldeab et al., 2007), while Heinrich Stadials (HS) have been invoked to explain millennial-scale dry periods in North Africa (Tjallingii et al., 2008), a delayed response of the East African monsoon to precession/insolation forcing (Ziegler et al., 2010a), as well as a southward shift in the Sahara-Sahel boundary (Collins et al., 2013). In particular, Ziegler et al. (2010a) proposed that African monsoon intensity (and by inference, sapropel formation) varies in phase with northern hemisphere summer insolation but was suppressed during Heinrich-type cold events, possibly associated with periods of meltwater release and sea-level rise. This suppression led to an apparent lag of the African monsoon behind insolation maxima. Ziegler et al. (2010a) proposed that this lag – while variable – averaged 2–3 kyr between precession minima and African monsoon maxima/sapropel mid-points. Our results for the Holocene and Last Interglacial support this hypothesis: S1 and S5 (and coeval increases in monsoon run-off) are preceded by North Atlantic cold events and meltwater pulses (dRSL > 0) (Fig. 9a,b), and the mid-points of these sapropels lag maximum insolation by 2–3 kyr (Fig. 7a,b). However, the relationship between these phenomena is not consistent for all sapropels/monsoon intervals. Meltwater pulses and North Atlantic cold events C21 and C24 preceded intervals of monsoon run-off and

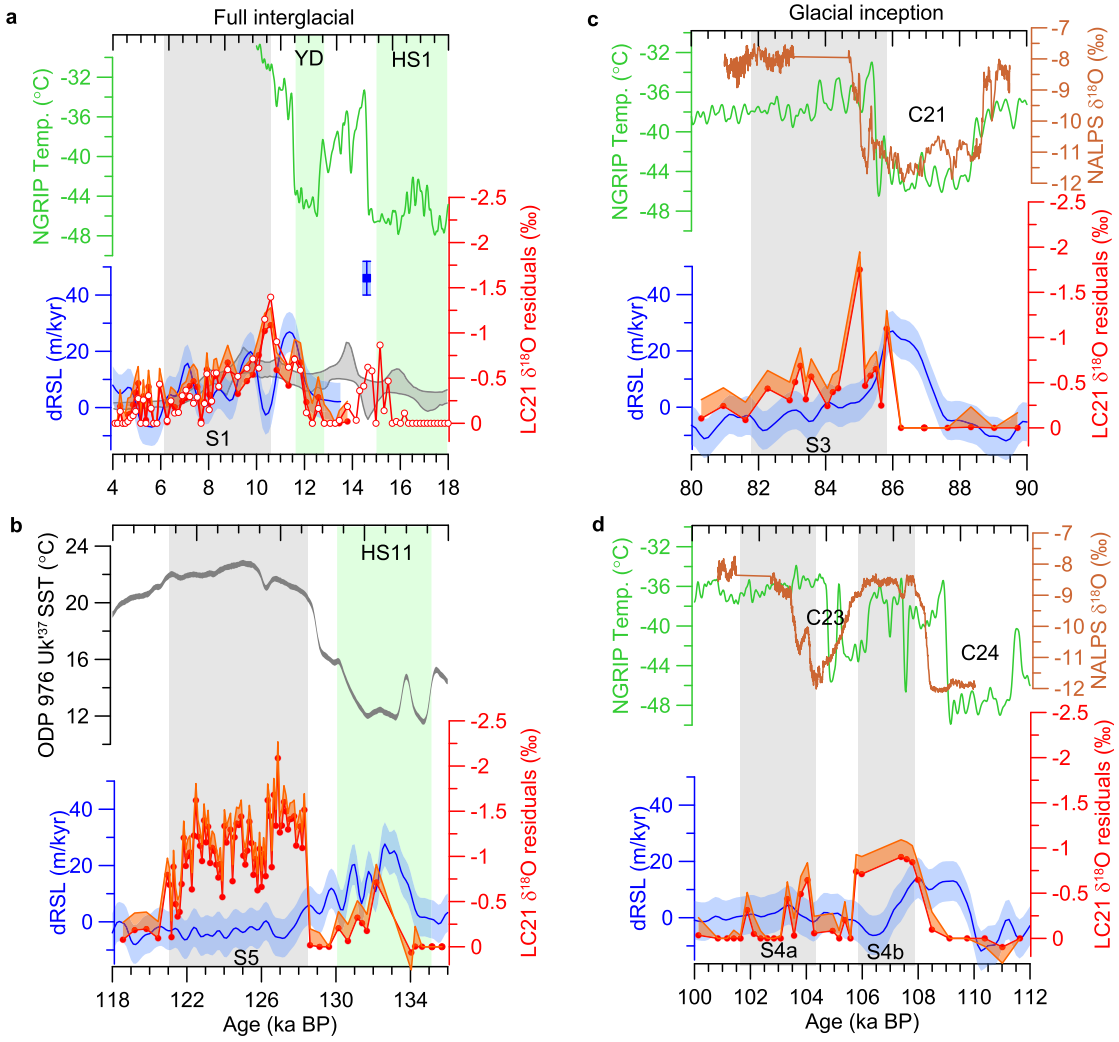

Fig. 9. Timing of North Atlantic cold events, meltwater events and East African monsoon maxima under full interglacial conditions (**a**, **b**) and periods of glacial inceptions (**c**, **d**). Cooling in the North Atlantic region is indicated by the NGRIP ice-core temperature record (green; Kindler et al., 2014) (**a**,**c**,**d**) and by a maximum probability, alkenone-derived sea surface temperature (SST) record from ODP Site 976 (**b**) (grey; Martrat et al., 2014) on a radiometric-based chronology (Marino et al., 2015). A U/Th-dated speleothem $\delta^{18}O$ record from the northern European Alps (NALPS; Boch et al., 2011), approximating Greenland temperature variations, is also shown (**c**,**d**). Cold events include the Younger Dryas (YD) (Rasmussen et al., 2014) and Heinrich Stadials 1 (Álvares-Solas et al., 2011) and 11 (Marino et al., 2015) (green rectangles), as well as events C21, C23, C24 (McManus et al., 1994). Meltwater events are inferred from rates of sea-level change (dRSL; blue) from Grant et al. (2012, 2014) (blue shading = 95% probability intervals of the maximum probability dRSL; line = maximum probability dRSL), and from Stanford et al. (2011) (grey shading in **a**; see Fig. 7). Also shown in (**a**) is MWP-1a at 46 m/kyr (Deschamps et al., 2012). LC21 residuals (red, orange) and sapropel intervals (grey rectangles) are the same as in Fig. 5.

sapropel deposition in the eastern Mediterranean during MIS 5a (sapropel S3) and 5c (sapropel S4), and cold event C23 interrupted S4 deposition (Fig. 9c,d), yet here the mid-point of these sapropels (and of the concurrent monsoon run-off intervals) is in direct phase with an insolation maximum. Hence, cold events and meltwater pulses do not necessarily induce a precession-lag in African monsoon/sapropel timing.

The maximum rates of sea-level rise prior to S3 are comparable to those for S5 (and for S1, if we consider the probabilistic dRSL records) (Fig. 9), implying that the rate of meltwater addition to the global ocean does not determine sapropel/monsoon lag. However, total sea-level change prior to S1 and S5 is tens of metres greater than for S3 and S4. If melting rates are comparable, this suggests that it is the duration of the meltwater addition that disrupts the precession-pacing of the African monsoon. Calculating from the start of the meltwater addition ('maximum probability' dRSL > 0) to the onset of monsoon run-off and sapropel deposition, we find meltwater durations of 7 kyr (for S5), 2 kyr (for S4) and 1.6 kyr (for S3) (Fig. 7). For S1, the Stanford et al. (2011) dRSL curve suggests that the main period of meltwater addition to the global ocean began ca 16.5–17 ka BP (Fig. 7a). This is consistent with a more recent estimate of 16.5 ka BP for the start of the main phase of deglaciation, although the initial phase began earlier (~20 ka BP) (Lambeck et al., 2014). Hence, the duration of meltwater addition prior to S1 was likely 6–9 kyr.

Modelling experiments suggest that the sensitivity of the AMOC and ITCZ (hence African monsoon precipitation) to meltwater pulses is greatest under full-glacial conditions (Ganopolski and Rahmstorf, 2001; Swingedouw et al., 2009; Zhang et al., 2015). Our African monsoon run-off reconstructions cover both glacial-inception and early interglacial periods, so it is unlikely that our observations primarily reflect climate-dependent sensitivities of the African monsoon. This gives further weight to our preferred interpretation that the duration of meltwater input to the global ocean was critical in determining the timing of the African monsoon response to insolation forcing. Interestingly, the inclusion of variable northern hemisphere ice sheets in transient model simulations of African monsoon variability (Ziegler et al., 2010b; Weber and Tuenter, 2011) produced zero phase lag in the precession band, in line with previous simulations based on stationary ice-sheets (Tuenter et al., 2005; Kutzbach et al., 2008). While Weber and Tuenter (2011) acknowledged that the crude resolution of ice sheets and ocean circulation, and lack of atmospheric mid-latitude dynamics in these transient models may undermine their reliability, these simulations are nonetheless quasi-consistent with our observations: we observe a tight phasing between sapropel mid-points (hence African monsoon intervals) and insolation maxima (= precession minima) in MIS 5a and 5c (Fig. 7c,d; Table 2). The fact that this observed phasing is not systematic among successive insolation maxima, may be the reason for model–data offsets if only 'average' phasings are considered. For example, lag correlation analyses (Caley et al., 2011) of a proxy record for African monsoon run-off into the eastern Mediterranean (Revel et al., 2010) revealed an average insolation-lag of 0.7 kyr for African monsoon maxima over the past 45 kyr, but a longer lag when the Holocene monsoon maximum was considered alone. Thus, statistical analyses may not capture the detail of monsoon–ice-volume phasings.

6. Conclusions

We have established independent (radiometric-based) datings for sapropels S1, S3, S4 and S5 in eastern Mediterranean core LC21, and show that, in detail, insolation–sapropel phasings were not systematic through the last glacial cycle. This observation potentially has implications for the application of an assumed 3-kyr lag between insolation maxima/precession minima and sapropel mid-points, and hence for the astronomical chronology of eastern Mediterranean sedimentary sequences. For instance, previous sapropel mid-point ages established by a lagged orbital tuning may be up to 3 kyr too young, in cases where the mid-points should actually be in direct phase (zero lag) with insolation maxima. However, it is unlikely that sapropel ages established by that method are too old. We suggest that persistent meltwater discharge into the North Atlantic over several kyrs, such as during glacial terminations, modified the timing of sapropel deposition via a delay in the timing of African monsoon run-off into the eastern Mediterranean. We show that the onset of this monsoon run-off and sapropel deposition was near-synchronous (within 0.5 kyr) for all sapropels considered here, and conclude that monsoon forcing was important in instigating the formation of these sapropels; furthermore, for sapropels S3–S5, monsoon forcing was probably more important than sea-level rise. However, it is likely that sea-level rise, and attendant hydrographic changes, strongly contributed to sapropel S1 deposition. Thus, deglaciation affected sapropel deposition directly (via changes in Mediterranean hydrography) and indirectly (via the response of the African monsoon to meltwater pulses). The fact that sapropel S1 was probably affected by both of the above mechanisms may explain why it exhibits the longest insolation lag compared to S3 to S5. That in turn would suggest that the 3-kyr lag assumption for sapropel tuning (which is based on S1) results in overestimated insolation lags for many sapropels. In this context, our observations may reconcile apparent model–data offsets with respect to the orbital pacing of the African monsoon, by demonstrating that insolation–monsoon phasings varied with the magnitude of meltwater pulses.

Finally, we conclude that deciphering the degree to which deep-water anoxia/sapropel deposition can be attributed to either sea-level rise or African monsoon run-off remains challenging, because both processes respond to boreal summer insolation, and both lead to a loss of surface buoyancy in the eastern Mediterranean and an attendant reduction in deep-water ventilation. This buoyancy sensitivity likely dates back to when the Mediterranean basin first became semi-enclosed from the open ocean during the Middle Miocene, which coincides with the first appearance of sapropels at ~15.4 Ma (Taylforth et al., 2014). Detailed process modelling of sapropels older than S1, and including the western Mediterranean basin, will help to elucidate how changes in sea level, SST, and monsoon run-off each contributed to Mediterranean palaeohydrography and sapropel formation.

Acknowledgements

This work was supported by Australian Research Council Australian Laureate Fellowship FL1201000050 (EJR), European Union FP7 project 298513 and Horizon 2020 project 655073 (MZ), and by the Deutsche Forschungsgemeinschaft project Kurzfristige Klimadynamik und biogeochemische Prozesse im Golf von Tarent: Von regionalen Proxyvariationen zu Klimazeitserien (UM). We thank two anonymous reviewers for their constructive comments.

References

Abouelmagd, A., Sultan, M., Milewski, A., Kehew, A.E., Sturchio, N.C., Soliman, F., Krishnamurthy, R.V., Cutrim, E., 2012. Toward a better understanding of palaeoclimatic regimes that recharged the fossil aquifers in North Africa: inferences from stable isotope and remote sensing data. Palaeogeogr. Palaeoclimatol. Palaeoecol. 329–330, 137–149.

Abouelmagd, A., Sultan, M., Sturchio, N.C., Soliman, F., Rashed, M., Ahmed, M., Kehew, A.E., Milewski, A., Chouinard, K., 2014. Paleoclimate record in the Nubian Sandstone Aquifer, Sinai Peninsula, Egypt. Quat. Sci. Rev. 81, 158–167.

Abu-Zied, R.H., Rohling, E.J., Jorissen, F.J., Fontanier, C., Casford, J.S.L., Cooke, S., 2008. Benthic foraminiferal response to changes in bottom water oxygenation and

organic carbon flux in the eastern Mediterranean during LGM to recent times. Mar. Micropaleontol. 67, 46–68.
Affek, H.P., Bar-Matthews, M., Ayalon, A., Matthews, A., Eiler, J.M., 2008. Glacial/interglacial temperature variations in Soreq cave speleothems as recorded by 'clumped isotope' thermometry. Geochim. Cosmochim. Acta 72, 5351–5360.
Almogi-Labin, A., Bar-Matthews, M., Shriki, D., Kolosovsky, E., Paterne, M., Schilman, B., Ayalon, A., Aizenshtat, Z., Matthews, A., 2009. Climatic variability during the last w90 ka of the southern and northern Levantine Basin as evident from marine records and speleothems. Quat. Sci. Rev. 28, 2882–2896.
Álvares-Solas, J., Montoya, M., Ritz, C., Ramstein, G., Charbit, S., Dumas, C., Nisancioglu, K., Dokken, T., Ganopolski, A., 2011. Heinrich event 1: an example of dynamical ice-sheet reaction to oceanic changes. Clim. Past 7, 1297–1306. http://dx.doi.org/10.5194/cp-7-1297-2011.
Bahr, A., Arz, H.W., Lamy, F., Wefer, G., 2006. Late glacial to Holocene paleoenvironmental evolution of the Black Sea, reconstructed with stable oxygen isotope records obtained on ostracod shells. Earth Planet. Sci. Lett. 241, 863–875.
Bahr, A., Lamy, F., Arz, H.W., Major, C., Kwiecien, O., Wefer, G., 2008. Abrupt changes of temperature and water chemistry in the late Pleistocene and early Holocene Black Sea. Geochem. Geophys. Geosyst. 9, Q01004. http://dx.doi.org/10.1029/2007GC001683.
Bar-Matthews, M., Ayalon, A., Gilmour, M., Matthews, A., Hawksesworth, C., 2003. Sea–land oxygen isotopic relationships from planktonic foraminifera and speleothems in the Eastern Mediterranean region and their implication for paleorainfall during interglacial intervals. Geochim. Cosmochim. Acta 67, 3181–3199.
Baumgartner, M., Kindler, P., Eicher, O., Floch, G., Schilt, A., Schwander, J., Spahni, R., Capron, E., Chappellaz, J., Leuenberger, M., Fischer, H., Stocker, T.F., 2014. NGRIP CH_4 concentration from 120 to 10 kyr before present and its relation to a $\delta^{15}N$ temperature reconstruction from the same ice core. Clim. Past 10, 903–920. http://dx.doi.org/10.5194/cp-10-903-2014.
Bazin, L., Landais, A., Lemieux-Dudon, B., Toyé Mahamadou Kele, H., Veres, D., Parrenin, F., Martinerie, P., Ritz, C., Capron, E., Lipenkov, V., Loutre, M.-F., Raynaud, D., Vinther, B., Svensson, A., Rasmussen, S.O., Severi, M., Blunier, T., Leuenberger, M., Fischer, H., Masson-Delmotte, V., Chappellaz, J., Wolff, E., 2013. An optimized multi-proxy, multi-site Antarctic ice and gas orbital chronology (AICC2012): 120–800 ka. Clim. Past 9, 1715–1731. http://dx.doi.org/10.5194/cp-9-1715-2013.
Béthoux, J.P., Pierre, C., 1999. Mediterranean functioning and sapropel formation: respective influences of climate and hydrological changes in the Atlantic and the Mediterranean. Mar. Geol 153, 29–39.
Bianchi, D., Zavatarelli, M., Pinardi, N., Capozzi, R., Capotondi, L., Corselli, C., Masina, S., 2006. Simulations of ecosystem response during the sapropel S1 deposition event. Palaeogeogr. Palaeoclimatol. Palaeoecol. 235, 265–287.
Boch, R., Cheng, H., Spötl, C., Edwards, R.L., Wang, X., Häuselmann, Ph., 2011. NALPS: a precisely dated European climate record 120–60 ka. Clim. Past 7, 1247–1259. http://dx.doi.org/10.5194/cp-7-1247-2011.
Bosmans, J.H.C., Drijfhout, S.S., Tuenter, E., Hilgen, F.J., Lourens, L.J., Rohling, E.J., 2015. Precession and obliquity forcing of the freshwater budget over the Mediterranean. Quat. Sci. Rev. 123, 16–30.
Bronk Ramsey, C., 2008. Deposition models for chronological records. Quat. Sci. Rev. 27, 42–60.
Bronk Ramsey, C., 2009. Bayesian analysis of radiocarbon dates. Radiocarbon 511, 337–360.
Bryden, H.L., Kinder, T.H., 1991. Steady two-layer exchange through the Strait of Gibraltar. Deep-Sea Res 38, S445–S463.
Cacho, I., Grimalt, J.O., Pelejero, C., Canals, M., Sierro, F.J., Flores, J.A., Shackleton, N., 1999. Dansgaard–Oeschger and Heinrich event imprints in Alboran Sea paleotemperatures. Paleoceanography 14, 698–705.
Caley, T., Malaizé, B., Revel, M., Ducassou, E., Wainer, K., Ibrahim, M., Shoeaib, D., Migeon, S., Marieu, V., 2011. Orbital timing of the Indian, East Asian and African boreal monsoons and the concept of a 'global monsoon'. Quat. Sci. Rev. 30, 3705–3715.
Capotondi, L., Principato, M.S., Morigi, C., Sangiorgi, F., Maffioli, P., Giunta, S., Negri, A., Corselli, C., 2006. Foraminiferal variations and stratigraphic implications to the deposition of sapropel S5 in the eastern Mediterranean. Palaeogeogr. Palaeoclimatol. Palaeoecol. 235, 48–65.
Casford, J.S.L., Rohling, E.J., Abu-Zied, R.H., Jorissen, F.J., Leng, M., Thomson, J., 2003. A dynamic concept for eastern Mediterranean circulation and oxygenation during sapropel formation. Palaeogeogr. Palaeoclimatol. Palaeoecol. 190, 103–119.
Casford, J.S.L., Abu-Zied, R., Rohling, E.J., Cooke, S., Fontanier, Ch., Leng, M., Millard, A., Thomson, J., 2007. A stratigraphically controlled multi-proxy chronostratigraphy for the eastern Mediterranean. Paleoceanography 22, PA4215. http://dx.doi.org/10.1029/2007PA001422.
Chang, P., Zhang, R., Hazeleger, W., Wen, C., Wan, X., Ji, L., Haarsma, R.J., Breugem, W.-P., Seidel, H., 2008. Oceanic link between abrupt changes in the North Atlantic Ocean and the African monsoon. Nat. Geosci. 1 (7), 444–448.
Chappellaz, J., Barnola, J.M., Raynaud, D., Korotkevich, Y.S., Lorius, C., 1990. Ice-core record of atmospheric methane over the past 160,000 years. Nature 345, 127–131.
Cita, M.B., Vergnaud-Grazzini, C., Robert, C., Chamley, H., Ciaranfi, N., d'Onofrio, S., 1977. Paleoclimatic record of a long deep sea core from the eastern Mediterranean. Quat. Res. 8, 205–235.
Collins, J.A., Govin, A., Mulitza, S., Heslop, D., Zabel, M., Hartmann, J., Röhl, U., Wefer, G., 2013. Abrupt shifts of the Sahara–Sahel boundary during Heinrich stadials. Clim. Past 9, 1181–1191. http://dx.doi.org/10.5194/cp-9-1181-2013.
Cramp, A., O'Sullivan, G., 1999. Neogene sapropels in the Mediterranean: a review. Mar. Geol. 153, 11–28.
De Lange, G.J., Thomson, J., Reitz, A., Slomp, C.P., Speranza Principato, M., Erba, E., Corselli, C., 2008. Synchronous basin-wide formation and redox-controlled preservation of a Mediterranean sapropel. Nat. Geosci. 1, 606–610.
de Noblet, N., Bracannot, P., Joussaume, S., Masson, V., 1996. Sensitivity of simulated Asian and African summer monsoons to orbitally induced variations in insolation 126, 115 and 6 kBP. Clim. Dyn 12, 589–603.
Deschamps, P., Durand, N., Bard, E., Hamelin, B., Camoin, G., Thomas, A.L., Henderson, G., Okuno, J., Yokoyama, Y., 2012. Ice-sheet collapse and sea-level rise at the Bølling warming 14,600 years ago. Nature 483, 559–564.
Dymond, J., Suess, E., Lyle, M., 1992. Barium in deep-sea sediment: a geochemical proxy for paleoproductivity. Paleoceanography 7, 163–181.
Emeis, K.-C., Robertson, A.H.F., Richter, C., Shipboard Scientific Party, 1996. Proceedings of the Ocean Drilling Program, Initial Reports, Leg 160. College Station, Texas.
Emeis, K.C., Struck, U., Schulz, H.M., Bernasconi, S., Sakamoto, T., Martinez-Ruiz, F., 2000. Temperature and salinity of Mediterranean Sea surface waters over the last 16,000 years: constraints on the physical environment of S1 sapropel formation based on stable oxygen isotopes and alkenone unsaturation ratios. Palaeogeogr. Palaeoclimatol. Palaeoecol. 158, 259–280.
Emeis, K.C., Schulz, H., Struck, U., Rossignol-Strick, M., Erlenkeuser, H., Howell, M.W., Kroon, D., Mackensen, H., Ishizuka, S., Oba, T., Sakamoto, T., Koizumi, I., 2003. Eastern Mediterranean surface water temperatures and $\delta^{18}O$ composition during deposition of sapropels in the late Quaternary. Paleoceanography 18. http://dx.doi.org/10.1029/2000PA000617.
Essallami, L., Sicre, M.A., Kallel, N., Siani, G., 2007. Hydrological changes in the Mediterranean Sea over the last 30,000 years. Geochem. Geophys. Geosyst. 8, 1–11.
Frumkin, A., Bar-Yosef, O., Schwarzc, H.P., 2011. Possible paleohydrologic and paleoclimatic effects on hominin migration and occupation of the Levantine Middle Paleolithic. J. Hum. Evol. 60, 437–451.
Ganopolski, A., Rahmstorf, S., 2001. Rapid changes of glacial climate simulated in a coupled climate model. Nature 409, 153–158.
Gasse, F., 2000. Hydrological changes in the African tropics since the last glacial maximum. Quat. Sci. Rev. 19, 189–211.
Grant, K.M., Rohling, E.J., Bar-Matthews, Ayalon, A., Bronk Ramsey, C.M., Satow, C., Medina-Elizalde, M., Roberts, A.P., 2012. Rapid coupling between ice volume and polar temperature over the past 150,000 years. Nature 491, 744–747.
Grant, K.M., Rohling, E.J., Bronk Ramsey, C., Cheng, H., Edwards, R.L., Florindo, F., Heslop, D., Marra, F., Roberts, A.P., Tamisiea, M.E., Williams, F., 2014. Sea-level variability over five glacial cycles. Nat. Commun. 5, 5076. http://dx.doi.org/10.1038/ncomms6076.
Grelaud, M., Marino, G., Ziveri, P., Rohling, E.J., 2012. Abrupt shoaling of the nutricline in response to massive freshwater flooding at the onset of the last interglacial sapropel event. Paleoceanography 27, PA3208. http://dx.doi.org/10.1029/2012PA002288.
Grimm, R., Maier-Reimer, E., Mikolajewicz, U., Schmiedl, G., Muller-Navarra, K., Adloff, F., Grant, K.M., Ziegler, M., Lourens, L.J., Emeis, K.C., 2015. Late glacial initiation of Holocene eastern Mediterranean sapropel formation. Nat. Commun. 6 http://dx.doi.org/10.1038/ncomms8099.
Hayes, A., Kucera, M., Kallel, N., Sbaffi, L., Rohling, E.J., 2005. Glacial Mediterranean sea surface temperatures reconstructed from planktonic foraminiferal assemblages. Quat. Sci. Rev. 24, 999–1016.
Hennekam, R., Jilbert, T., Schnetger, B., de Lange, G.J., 2014. Solar forcing of Nile discharge and sapropel S1 formation in the early to middle Holocene eastern Mediterranean. Paleoceanography 29. http://dx.doi.org/10.1002/2013PA002553.
Higgs, N.C., Thomson, J., Wilson, T.R.S., Croudace, I.W., 1994. Modification and complete removal of eastern Mediterranean sapropels by postdepositional oxidation. Geology 22, 423–426.
Hilgen, F.J., Lourens, L.J., Berger, A., Loutre, M.F., 1993. Evaluation of the astronomically calibrated time scale for the late Pliocene and earliest Pleistocene. Paleoceanography 8, 549–565.
Hughes, P.D., Woodward, J.C., Gibbard, P.L., 2006. Quaternary glacial history of the Mediterranean mountains. Prog. Phys. Geogr. 30, 334–364.
Hughes, P.D., Woodward, J.C., 2009. Glacial and periglacial environments. In: Woodward, J.C. (Ed.), The Physical Geography of the Mediterranean. Oxford University Press, ISBN 978-0-19-926803-0, pp. 33–67.
Jimenez-Amat, P., Zahn, R., 2015. Offset timing of climate oscillations during the last two glacial-interglacial transitions connected with large-scale freshwater perturbation. Paleoceanography 30. http://dx.doi.org/10.1002/2014PA002710.
Jorissen, F.J., 1999. Benthic foraminiferal successions across Late Quaternary Mediterranean sapropels. Mar. Geol. 153, 91–101.
Kageyama, M., Merkel, U., Otto-Bliesner, B., Prange, M., Abe-Ouchi, A., Lohmann, G., Ohgaito, R., Roche, D.M., Singarayer, J., Swingedouw, D., Zhang, X., 2013. Climatic impacts of fresh water hosing under Last Glacial Maximum conditions: a multi-model study. Clim. Past 9, 935–953. http://dx.doi.org/10.5194/cp-9-935-2013.
Kallel, N., Paterne, M., Duplessy, J.C., Vergnaud-Grazzini, C., Pujol, C., Labeyrie, L., Arnold, M., Fontugne, M., Pierre, C., 1997. Enhanced rainfall in the Mediterranean region during the last sapropel event. Oceanol. Acta 20, 697–712.
Kallel, N., Duplessy, J.C., Labeyrie, L., Fontugne, M., Paterne, M., Montacer, M., 2000. Mediterranean pluvial periods and sapropel formation over the last 200 000

years. Palaeogeogr. Palaeoclimatol. Palaeoecol. 157, 45–58.
Kandiano, E.S., Bauch, H.A., Fahl, K., 2014. Last interglacial surface water structure in the western Mediterranean (Balearic) Sea: climatic variability and link between low and high latitudes. Glob. Planet. Change 123, 67–76.
Kindler, P., Guillevic, M., Baumgartner, M., Schwander, J., Landais, A., Leuenberger, M., 2014. Temperature reconstruction from 10 to 120 kyr b2k from the NGRIP ice core. Clim. Past 10, 887–902. http://dx.doi.org/10.5194/cp-10-887-2014.
Kolodny, Y., Stein, M., Machlus, M., 2005. Sea-rain-lake relation in the Last Glacial East Mediterranean revealed by $\delta^{18}O$–$\delta^{13}C$ in Lake Lisan aragonites. Geochim. Cosmochim. Acta 69, 4045–4060.
Kullenberg, B., 1952. On the salinity of the water contained in marine sediments. Medd. Oceanogr. Inst. Göteb. 21, 1–38.
Kutzbach, J.E., Liu, X., Liu, Z., Chen, G., 2008. Simulation of the evolutionary response of global summer monsoons to orbital forcing over the past 280,000 years. Clim. Dyn. 30, 567–579.
Lambeck, K., Rouby, H., Purcell, A., Sun, Y., Sambridge, M., 2014. Sea level and global ice volumes from the Last Glacial Maximum to the Holocene. Proc. Natl. Acad. Sci. U. S. A. 111 (43), 15296–15303. http://dx.doi.org/10.1073/pnas.1411762111.
Langgut, D., Almogi-Labin, A., Bar-Matthews, M., Weinstein-Evron, M., 2011. Vegetation and climate changes in the South Eastern Mediterranean during the Last Glacial-Interglacial cycle (86 ka): new marine pollen record. Quat. Sci. Rev. 30, 3960–3972.
Larrasoaña, J.C., Roberts, A.P., Rohling, E.J., Winklhofer, M., Wehausen, R., 2003. Three million years of monsoon variability over the northern Sahara. Clim. Dyn. 21, 689–698.
Laskar, J., 1990. The chaotic motion of the solar system: a numerical estimate of the size of the chaotic zones. Icarus 88, 266–291.
Lézine, A.-M., Hély, C., Grenier, C., Braconnot, P., Krinner, G., 2011. Sahara and Sahel vulnerability to climate changes, lessons from Holocene hydrological data. QSR 30, 3001–3012.
Lombo Tombo, S., Dennielou, B., Berné, S., Bassetti, M.-A., Toucanne, S., Jorry, S.J., Jouet, G., Fontanier, C., 2015. Sea-level control on turbidite activity in the Rhone canyon and the upper fan during the Last Glacial Maximum and Early deglacial. Sediment. Geol. 323, 148–166.
Lourens, L.J., Antonarakou, A., Hilgen, F.J., van Hoof, A.A.M., Vergnaud-Grazzini, C., Zachariasse, W.J., 1996. Evaluation of the Plio-Pleistocene astronomical timescale. Paleoceanography 11, 391–413.
Lourens, L.J., Hilgen, F., Shackleton, N.J., Laskar, J., Wilson, D., 2004. The Neogene period. In: Gradstein, F.M., Ogg, J.G., Smith, A.G. (Eds.), A Geologic Timescale 2004. Cambridge University Press, pp. 409–440.
Major, C.O., Goldstein, S.L., Ryan, W.B.F., Lericolais, G., Piotrowski, A.M., Hajdas, I., 2006. The co-evolution of Black Sea level and composition through the last deglaciation and its paleoclimatic significance. Quat. Sci. Rev. 25, 2031–2047.
Marino, G., Rohling, E.J., Rijpstra, W.I., Sangiorgi, F., Schouten, S., Sinninghe Damsté, J.S., 2007. Aegean Sea as driver for hydrological and ecological changes in the eastern Mediterranean. Geology 35, 675–678.
Marino, G., Rohling, E.J., Sangiorgi, F., Hayes, A., Casford, J.S.L., Lotter, A.F., Kucera, M., Brinkhuis, H., 2009. Early and middle Holocene in the Aegean Sea: interplay between high and low latitude climate variability. Quat. Sci. Rev. 28, 3246–3262.
Marino, G., Rohling, E.J., Rodríguez-Sanz, L., Grant, K.M., Heslop, D., Roberts, A.P., Stanford, J.D., Yu, J., 2015. Bipolar seesaw control on last interglacial sea level. Nature 522, 197–201.
Martrat, B., Jiminez-Amat, P., Zahn, R., Grimalt, J.O., 2014. Similarities and dissimilarities between the last two deglaciations and interglaciations in the North Atlantic region. Quat. Sci. Rev 99, 122–134.
Marzin, C., Braconnot, P., Kageyama, M., 2013. Relative impacts of insolation changes, meltwater fluxes and ice sheets on African and Asian monsoons during the Holocene. Clim. Dyn. 41, 2267–2286.
Matthews, A., Ayalon, A., Bar-Matthews, M., 2000. D/H ratios of fluid inclusions of Soreq Cave (Israel) speleothems as a guide to the Eastern Mediterranean Meteoric Line relationships in the last 120 ky. Chem. Geol. 166, 183–191.
McGarry, S., Bar-Matthews, M., Matthews, A., Vaks, A., Schilman, B., Ayalon, A., 2004. Constraints on hydrological and paleotemperature variations in the Eastern Mediterranean region in the last 140 ka given by the δD values of speleothem fluid inclusions. Quat. Sci. Rev. 23, 919–934.
McManus, J.F., Bond, G.C., Broecker, W.S., Johnsen, S., Labeyrie, L., Higgins, S., 1994. High-resolution climate records from the N. Atlantic during the last interglacial. Nature 371, 326–329.
Melki, T., Kallel, N., Jorissen, F.J., Guichard, J.F., Dennielou, B., Berné, S., Labeyrie, L., Fontugne, M., 2009. Abrupt climate change, sea surface salinity and paleoproductivity in the western Mediterranean Sea (Gulf of Lion) during the last 28 kyr. Palaeogeogr. Palaeoclimatol. Palaeoecol. 279, 96–113.
Mercone, D., Thomson, J., Croudace, I.W., Siani, G., Paterne, M., Troelstra, S., 2000. Duration of S1, the most recent Mediterranean sapropel, as indicated by AMS radiocarbon and geochemical evidence. Paleoceanography 15, 336–347.
Mercone, D., Thomson, J., Abu-Zied, R.H., Croudace, I.W., Rohling, E.J., 2001. High-resolution geochemical and micropalaeontological profiling of the most recent eastern Mediterranean sapropel. Mar. Geol. 177, 25–44.
Milner, A.M., Collier, R.E.L., Roucoux, K.H., Müller, U.C., Pross, J., Kalaitzidis, S., Christanis, K., Tzedakis, P.C., 2012. Enhanced seasonality of precipitation in the Mediterranean during the early part of the Last Interglacial. Geology 40, 919–922.
Nicholson, S.E., 2009. A revised picture of the structure of the "monsoon" and land ITCZ over West Africa. Clim. Dyn. 32, 1155–1171. http://dx.doi.org/10.1007/s00382-008-0514-3.
Nijenhuis, I.A., Bosch, H.J., Sinnighe Damsté, J.S., Brumsack, H.-J., de Lange, G.J., 1999. Organic matter and trace element rich sapropels and black shales: a geochemical comparison. Earth Planet. Sci. Lett. 169, 277–290.
Olausson, E., 1961. Studies of Deep-sea Cores. In: Reports of the Swedish Deep Sea Expedition 1947–1948, 8, pp. 353–391.
Osborne, A.H., Vance, D., Rohling, E.J., Barton, N., Rogerson, M., Fello, N., 2008. A humid corridor across the Sahara for the migration "Out of Africa" of early modern humans 120,000 years ago. Proc. Natl. Acad. Sci. U. S. A. 105, 16444–16447.
Osborne, A., Marino, G., Vance, D., Rohling, E.J., 2010. Eastern Mediterranean surface water Nd during Eemian sapropel S5: monitoring northerly (mid latitude) versus southerly (sub tropical) freshwater contributions. Quat. Sci. Rev. 29, 2473–2483.
Otto-Bliesner, B.L., Russell, J.M., Clark, P.U., Liu, Z., Overpeck, J.T., Konecky, B., deMenocal, P., Nicholson, S.E., He, F., Lu, Z., 2014. Coherent changes of southeastern equatorial and northern African rainfall during the last deglaciation. Science 346, 1223–1227.
Pinardi, N., Bonaduce, A., Navarra, A., Dobricic, S., Oddo, P., 2014. The mean sea level equation and its application to the Mediterranean Sea. J. Clim. 27, 442–447.
Rasmussen, S.O., Bigler, M., Blockley, S.P., Blunier, T., Buchardt, S.L., Clausen, H.B., Cvijanovic, I., Dahl-Jensen, D., Johnsen, S.J., Fischer, H., Gkinis, V., 2014. A stratigraphic framework for abrupt climatic changes during the Last Glacial period based on three synchronized Greenland ice-core records: refining and extending the INTIMATE event stratigraphy. Quat. Sci. Rev. 106, 14–28.
Revel, M., Ducassou, E., Grousset, F.E., Bernasconi, S.M., Migeon, S., Revillon, S., Mascle, J., Murat, A., Zaragosi, S., Bosch, D., 2010. 100,000 years of African monsoon variability recorded in sediments of the Nile margin. Quat. Sci. Rev. 29, 1342–1362.
Rogerson, M., Colmenero-Hidalgo, E., Levine, R.C., Rohling, E.J., Voelker, A.H.L., Bigg, G.R., Schönfeld, J., Cacho, I., Sierro, F.J., Löwemark, L., Reguera, M.I., deAbreu, L., Garrick, K., 2010. Enhanced Mediterranean-Atlantic exchange during Atlantic freshening phases. Geochem. Geophys. Geosyst. 11, Q08013. http://dx.doi.org/10.1029/2009GC002931.
Rogerson, M., Rohling, E.J., Bigg, G.R., Ramirez, J., 2012. Palaeoceanography of the Atlantic-Mediterranean Exchange: overview and first quantitative assessment of climatic forcing. Rev. Geophys 50. RG2003. http://dx.doi.org/10.1029/2011RG000376.
Rohling, E.J., 1994. Review and new aspects concerning the formation of Mediterranean sapropels. Mar. Geol. 122, 1–28.
Rohling, E.J., 1999. Environmental control on Mediterranean salinity and $\delta^{18}O$. Paleoceanography 14, 706–715.
Rohling, E.J., 2013. Quantitative assessment of glacial fluctuations in the level of Lake Lisan, Dead Sea rift. Quat. Sci. Rev. 70, 63–72.
Rohling, E.J., Gieskes, W.W.C., 1989. Late quaternary changes in Mediterranean intermediate water density and formation rate. Paleoceanography 4, 531–545.
Rohling, E.J., Bryden, H.L., 1994. Estimating past changes in the eastern Mediterranean freshwater budget, using reconstructions of sea level and hydrography. Proc. K. Ned. Akad. Wet. Ser. B 97, 201–217.
Rohling, E.J., De Rijk, S., 1999. The Holocene climate optimum and last glacial maximum in the Mediterranean: the marine oxygen isotope record. Mar. Geol. 153, 57–75.
Rohling, E.J., Cane, T.R., Cooke, S., Sprovieri, M., Bouloubassi, I., Emeis, K.C., Schiebel, R., Kroon, D., Jorissen, F.J., Lorre, A., Kemp, A.E.S., 2002. African monsoon variability during the previous interglacial maximum. Earth Planet. Sci. Lett. 202, 61–75.
Rohling, E.J., Sprovieri, M., Cane, T.R., Casford, J.S.L., Cooke, S., Bouloubassi, I., Emeis, K.C., Schiebel, R., Hayes, A., Jorissen, F.J., Kroon, D., 2004. Reconstructing past planktic foraminiferal habitats using stable isotope data: a case history for Mediterranean sapropel S5. Mar. Micropaleontol. 50, 89–123.
Rohling, E.J., Hopmans, E.C., Sinninghe-Damsté, J.S., 2006. Water column dynamics during the last interglacial anoxic event in the Mediterranean (sapropel S5). Paleoceanography 21, PA2018. http://dx.doi.org/10.1029/2005PA001237.
Rohling, E.J., Grant, K., Bolshaw, M., Roberts, A.P., Siddall, M., Hemleben, Ch, Kucera, M., 2009. Antarctic temperature and global sea level closely coupled over the past five glacial cycles. Nat. Geosci. 2, 500–504.
Rohling, E.J., Foster, G.L., Grant, K.M., Marino, G., Roberts, A.P., Tamisiea, M.E., Williams, F., 2014. Sea-level and deep-sea-temperature variability over the past 5.3 million years. Nature 508, 477–482.
Rohling, E.J., Marino, G., Grant, K., 2015. Mediterranean climate and oceanography, and the periodic development of anoxic events (sapropels). Earth-Sci. Rev. 143, 62–97.
Rossignol-Strick, M., 1985. Mediterranean quaternary sapropels, an immediate response of the African monsoon to variation of insolation. Palaeogeogr. Palaeoclimatol. Palaeoecol. 49, 237–263.
Rossignol-Strick, M., 1987. Rainy periods and bottom water stagnation initiating brine accumulation and metal concentrations: 1. The Late Quaternary. Paleoceanography 2, 333–360.
Rossignol-Strick, M., 1999. The Holocene climatic optimum and pollen records of sapropel 1 in the eastern Mediterranean, 9000–6000 BP. Quat. Sci. Rev. 18, 515–530.
Rossignol-Strick, M., Paterne, M., 1999. A synthetic pollen record of the eastern Mediterranean sapropels of the last 1 Ma: implications for the time-scale and formation of sapropels. Mar. Geol. 153, 221–237.

Rossignol-Strick, M., Nesteroff, W., Olive, P., Vergnaud-Grazzini, C., 1982. After the deluge, Mediterranean stagnation and sapropel formation. Nature 295, 105–110.
Ryan, W.B.F., 1972. Stratigraphy of late quaternary sediments in the Eastern Mediterranean. In: Stanley, D.J. (Ed.), The Mediterranean Sea Strasbourg, Va. (Dowden, Hutchinson and Ross), p. 765.
Satow, C., Tomlinson, E.L., Grant, K.M., Albert, P.G., Smith, V.C., Manning, C.J., Ottolini, L., Wulf, S., Rohling, E.J., Lowe, J.J., Blockley, S.P.E., Menzies, M.A., 2015. A new contribution to the Late Quaternary tephrostratigraphy of the Mediterranean: Aegean Sea core LC21. Quat. Sci. Rev. 117, 96–112.
Schilt, A., Buiron, D., Capron, E., Chappellaz, J., Loulergue, L., Spahni, R., Stocker, T.F., 2010. EPCIA Dronning Maud Land Ice Core CH_4 Data to 140 kyr BP. IGBP PAGES/World Data Center for Paleoclimatology Data Contribution Series # 2010-131. NOAA/NCDC Paleoclimatology Program, Boulder CO, USA.
Schmiedl, G., Mitschele, A., Beck, S., Emeis, K.C., Hemleben, Ch., Schultz, H., Sperling, M., Weldeab, S., 2003. Benthic foraminiferal record of ecosystem variability in the eastern Mediterranean Sea during times of sapropel S5 and S6 deposition. Palaeogeogr. Palaeoclimatol. Palaeoecol. 190, 139–164.
Schmiedl, G., Kuhnt, T., Ehrmann, W., Emeis, K.-C., Hamann, Y., Kotthoff, U., Dulski, P., Pross, J., 2010. Climatic forcing of eastern Mediterranean deep-water formation and benthic ecosystems during the past 22 000 years. Quat. Sci. Rev 29, 3006–3020.
Scrivner, A.E., Vance, D., Rohling, E.J., 2004. New neodymium isotope data quantify Nile involvement in Mediterranean anoxic episodes. Geology 32, 565–568.
Siddall, M., Rohling, E.J., Almogi-Labin, A., Hemleben, Ch., Meischner, D., Schmeltzer, I., Smeed, D.A., 2003. Sea-level fluctuations during the last glacial cycle. Nature 423, 853–858.
Siddall, M., Smeed, D.A., Hemleben, Ch., Rohling, E.J., Schmeltzer, I., Peltier, W.R., 2004. Understanding the Red Sea response to sea level. Earth Planet. Sci. Lett. 225, 421–434.
Sierro, F.J., Hodell, D.A., Curtis, J.H., Flores, J.A., Reguera, I., Colmenero-Hidagalo, E., Barcena, M.A., Grimalt, J.O., Cacho, I., Frigola, J., Canals, M., 2005. Impact of iceberg melting on Mediterranean thermohaline circulation during Heinrich events. Paleoceanography 20, 1–13.
Soulet, G., Ménot, G., Bayon, G., Rostek, F., Ponzevera, E., Toucanne, S., Lericolais, G., Bard, E., 2013. Abrupt drainage cycles of the Fennoscandian Ice Sheet. Proc. Natl. Acad. Sci. U. S. A. 110, 6682–6687.
Spahni, R., Wania, R., Neef, L., van Weele, M., Pison, I., Bousquet, P., Frankenberg, C., Foster, P.N., Joos, F., Prentice, I.C., van Velthoven, P., 2011. Constraining global methane emissions and uptake by ecosystems. Biogeosciences 8, 1643–1665. http://dx.doi.org/10.5194/bg-8-1643-2011.
Sperling, M., Schmiedl, G., Hemleben, Ch., Emeis, K.C., Erlenkeuser, H., Grootes, P.M., 2003. Black Sea impact on the formation of eastern Mediterranean sapropel S1? Evidence from the Marmara Sea. Palaeogeogr. Palaeoclimatol. Palaeoecol. 190, 9–21.
Stanford, J.D., Hemingway, R., Rohling, E.J., Challenor, P.G., Medina-Elizalde, M., Lester, A.J., 2011. Sea-level probability for the last deglaciation: a statistical analysis of far-field records. Glob. Planet. Change 79, 193–203.
Swingedouw, D., Mignot, J., Braconnot, P., Mosquet, E., Kageyama, M., Alkama, R., 2009. Impact of freshwater release in the North Atlantic under different climate conditions in an OAGCM. J. Clim. 22, 6377–6403.
Swingedouw, D., Rodehacke, C.B., Behrens, E., Menary, M., Olsen, S.M., Gao, Y., Mikolajewicz, U., Mignot, J., Biastoch, A., 2013. Decadal fingerprints of freshwater discharge around Greenland in a multi-model ensemble. Clim. Dyn. 41 (3–4), 695–720.
Taylforth, J.E., McCay, G.A., Ellam, R., Raffi, I., Kroon, D., Robertson, A.H.F., 2014. Middle Miocene (Langhian) sapropel formation in the easternmost Mediterranean deep-water basin: evidence from northern Cyprus. Mar. Pet. Geol. 57, 521–536.
Thomson, J., Higgs, N.C., Wilson, T.R.S., Croudace, I.W., De Lange, G.J., van Santvoort, P.J.M., 1995. Redistribution and geochemical behaviour of redox sensitive elements around S1, the most recent eastern Mediterranean sapropel. Geochim. Cosmochim. Acta 59, 3487–3501.
Thomson, G., Mercone, D., de Lange, G.J., van Santvoort, P.J.M., 1999. Review of recent advances in the interpretation of eastern Mediterranean sapropel S1 from geochemical evidence. Mar. Geol. 153, 77–89.
Thomson, J., Crudeli, D., De Lange, G.J., Slomp, C.P., Erba, E., Corselli, C., Calvert, S.E., 2004. Florisphaera profunda and the origin and diagenesis of carbonate phases in eastern Mediterranean sapropel units. Paleoceanography 19, PA3003. http://dx.doi.org/10.1029/2003PA000976.
Tjallingii, R., Claussen, M., Stuut, J.-B.W., Fohlmeister, J., Jahn, A., Bickert, T., Lamy, F., Rohl, U., 2008. Coherent high- and low-latitude control of the northwest African hydrological balance. Nat. Geosci. 1, 670–675.
Toucanne, S., Soulet, G., Freslon, N., Silva Jacinto, R., Dennielou, B., Zaragosi, S., Eynaud, F., Bourillet, J.-F., Bayon, G., 2015a. Millennial-scale fluctuations of the European Ice Sheet at the end of the last glacial, and their potential impact on global climate. Quat. Sci. Rev. 123, 113–133.
Toucanne, S., Minto'o, C.M.A., Fontanier, C., Bassetti, M.A., Jorry, S.J., Jouet, G., 2015b. Tracking rainfall in the northern Mediterranean borderlands during sapropel deposition. Quat. Sci. Rev. 129, 178–195.
Troelstra, S.R., Ganssen, G.M., Van der Borg, K., De Jong, A.F.M., 1991. A Late Quaternary stratigraphic framework for eastern Mediterranean sapropel S1 based on AMS ^{14}C dates and stable isotopes. Radiocarbon 33, 15–21.
Tuenter, E., Weber, S.L., Hilgen, F.J., Lourens, L.J., Ganopolski, A., 2005. Simulation of climate phase lags in response to precession and obliquity forcing and the role of vegetation. Clim. Dyn. 24, 279–295.
Tzedakis, P.C., 2007. Seven ambiguities in the Mediterranean palaeoenvironmental narrative. Quat. Sci. Rev. 26, 2042–2066.
Tzedakis, P.C., 2009. Cenozoic climate and vegetation change. In: Woodward, J.C. (Ed.), The Physical Geography of the Mediterranean. Oxford University Press, Oxford, pp. 89–137.
Tzedakis, P.C., Lawson, I.T., Frogley, M.R., Hewitt, G.M., Preece, R.C., 2002. Buffered vegetation changes in a Quaternary refugium: evolutionary implications. Science 297, 2044–2047.
Tzedakis, P.C., Frogley, M.R., Heaton, T.H.E., 2003. Last interglacial conditions in southern Europe: evidence from Ioannina, northwest Greece. Glob. Planet. Change 36, 157–170.
Vaks, A., Bar-Matthews, M., Ayalon, A., Matthews, A., Frumkin, A., Dayan, U., Halicz, L., Almogi-Laban, A., Schilman, B., 2006. Paleoclimate and location of the border between Mediterranean climate region and the Saharo–Arabian Desert as revealed by speleothems from the northern Negev Desert, Israel. Earth Planet. Sci. Lett. 249, 384–399.
Voelker, A.H.L., Lebreiro, S.M., Schöfeld, J., Cacho, I., Erlenkeuser, H., Abrantes, F., 2006. Mediterranean outflow strengthening during northern hemisphere coolings: a salt source for the glacial Atlantic? Earth Planet. Sci. Lett. 245, 39–55.
Weber, S.L., Tuenter, E., 2011. The impact of varying ice sheets and greenhouse gases on the intensity and timing of boreal summer monsoons. Quat. Sci. Rev. 30, 469–479.
Weldeab, S., Lea, D.W., Schneider, R.R., Andersen, N., 2007. 155,000 years of West African monsoon and ocean thermal evolution. Science 316, 1303–1307.
Wijmstra, T.A., Young, R., Witte, H.J.L., 1990. An evaluation of the climatic conditions during the Late Quaternary in northern Greece by means of multivariate analysis of palynological data and comparison with recent phytosociological and climatic data. Geol. Mijnb. 69, 243–251.
Zhang, X., Prange, M., Merkel, U., Schulz, M., 2015. Spatial fingerprint and magnitude of changes in the Atlantic meridional overturning circulation during marine isotope stage 3. Geophys. Res. Lett. 42, 1903–1911. http://dx.doi.org/10.1002/2014GL063003.
Ziegler, M., Tuenter, E., Lourens, L.J., 2010a. The precession phase of the boreal summer monsoon as viewed from the eastern Mediterranean (ODP Site 968). Quat. Sci. Rev. 29, 1481–1490.
Ziegler, M., Lourens, L.J., Tuenter, E., Hilgen, F.J., Reichart, G.J., Weber, S.L., 2010b. Precession phase offset between Arabian Sea biological productivity and the Indian summer monsoon. Paleoceanography 25, PA3213. http://dx.doi.org/10.1029/2009PA001884.